Published in final edited form as:
EMBO J. 2018 March 15; 37(6): . doi:10.15252/embj.201797822.

Prion-like protein aggregates exploit the RHO to cofilin-1 signaling pathway to enter cells

Zhen Zhong, **Laura Grasso**[#], **Caroline Sibilla**[#], **Tim Stevens**, **Nicholas Barry**, and **Anne Bertolotti**[*]
MRC Laboratory of Molecular Biology, Francis Crick Avenue, Cambridge, CB2 0QH, United Kingdom

[#] These authors contributed equally to this work.

Abstract

Protein aggregation is a hallmark of diverse neurodegenerative diseases. Multiple lines of evidence have revealed that protein aggregates can penetrate inside cells and spread like prions. How such aggregates enter cells remains elusive. Through a focused siRNA screen targeting genes involved in membrane trafficking, we discovered that mutant SOD1 aggregates, like viruses, exploit cofilin-1 to remodel cortical actin and enter cells. Upstream of cofilin-1, signaling from the RHO GTPase and the ROCK1 and LIMK1 kinases controls cofilin-1 activity to remodel actin and modulate aggregate entry. In the spinal cord of symptomatic $SOD1^{G93A}$ transgenic mice, cofilin-1 phosphorylation is increased and actin dynamic altered. Importantly, the RHO to cofilin-1 signaling pathway also modulates entry of Tau and α-synuclein aggregates. Our results identify a common host cell signaling pathway that diverse protein aggregates exploit to remodel actin and enter cells.

Keywords

Prions; aggregation; neurodegenerative diseases; spreading of aggregation; actin; cofilin

Introduction

The deposition of proteins of abnormal conformation is at the origin of a broad range of human age-related diseases including the devastating neurodegenerative diseases Alzheimer's (AD), Parkinson's (PD), Huntington's (HD), Amyotrophic Lateral Sclerosis (ALS), dementia and prion diseases (Soto, 2003). Prion diseases were traditionally thought to be unique because the misfolded protein in this group of diseases, PrP, is infectious

[*]Correspondence: aberto@mrc-lmb.cam.ac.uk.

Authors contributions

A.B. conceived, directed the study and wrote the manuscript. Z.Z. conceived and performed experiments, prepared the figures and help writing the manuscript. N.B. and Z.Z. developed imaging method and N.B. assisted with confocal microscopy. T.J.S. provided computational biology support and performed the statistical analysis in the screen. C.S. contributed to SOD1 protein purification and SOD1 aggregate characterization. L.G. performed the additional experiments required for the revision.

Conflict of interest

The authors declare no conflict of interest.

Europe PMC Funders Author Manuscripts

(Prusiner, 1998). A prion is a proteinaceous infectious particle which can enter cells and propagate its misfolded and pathogenic conformation by corrupting the normally soluble host protein. In the recent years, an explosion of studies has challenged our views on neurodegenerative diseases. In fact, the diverse protein aggregates that characterize neurodegenerative diseases share the defining properties of prions and can spread their abnormal conformation like prions, where seeds made of protein aggregates can induce aggregation of the soluble counterpart in a host (Jucker & Walker, 2011; Brundin *et al*, 2010; Frost & Diamond, 2010; Munch & Bertolotti, 2012; Prusiner, 2012). Therefore, knowledge on the extremely rare prion diseases has opened up new avenues for the understanding of more common neurodegenerative diseases such as AD or ALS.

Amongst the diverse neurodegenerative diseases, ALS is an attractive model to study the propagation of protein aggregates because its defining clinical features are reminiscent of prion diseases. Like prion diseases, ALS is a devastating and rapidly progressive neurodegenerative disease. ALS manifests by muscle weakness, which always begins at a focal point, but the body region involved is highly variable between individuals. The symptoms then spread contiguously to adjacent regions by an orderly process (Gowers, 1892; Ravits & La Spada, 2009). The spreading of SOD1 aggregates from cell to cell by a prion-like mechanism, which has not only been observed in cells (Münch *et al*, 2011; Grad *et al*, 2011; 2014) but also in mice (Ayers *et al*, 2014; 2015; Thomas *et al*, 2017), could explain the defining pathological hallmarks of ALS. With this model, the site of disease corresponds to the misfolding of the disease-causing protein and the spreading of the symptoms results from the spreading of the SOD1 prion.

Numerous studies have demonstrated the propagation of diverse disease-related protein aggregates in animal models (Sibilla & Bertolotti, 2017). However, the mechanisms underlying these properties are largely unknown. Cellular models recapitulating the propagation of protein aggregates are essential to conduct mechanistic studies. In most cases, the protein aggregates associated with neurodegenerative diseases are intracellular and replicate inside cells. Therefore, amongst the diverse steps of the prion cycle, the entry of protein aggregates into their host is a particularly important one because it is a first step in a pathological cascade and so far, this process is ill-defined.

We have previously shown that SOD1 aggregates enter cells by macropinocytosis (Münch *et al*, 2011), a route later found to be also exploited by Tau aggregates (Holmes *et al*, 2013). Here we aimed at identifying cellular factors involved in aggregate entry. Knowing that aggregates enter cells by macropinocytosis, a poorly defined endocytic pathway, we designed a targeted siRNA screen using a membrane trafficking siRNA library to identify host cell factors involved in aggregate entry, with the hope to provide some mechanistic insights in this elusive prion-like cycle.

Our work identifies a critical cellular factor, cofilin-1 required to remodel cortical actin, enabling entry of diverse protein aggregates. Upstream of cofilin-1 and controlling aggregate entry is the RHO-ROCK1-LIMK1 signaling pathway. These findings reveal host cellular factors critical for aggregate entry. Remarkably, cofilin-1 is also exploited by some viruses

to enter cells, thereby highlighting an analogy between entry of protein aggregates and viruses.

Results

An siRNA screen identifies modifiers of mutant SOD1 aggregate uptake

We previously found that SOD1 aggregates enter cells by macropinocytosis (Münch *et al*, 2011), a finding confirmed by others (Zeineddine *et al*, 2015) and relevant to diverse disease-causing aggregates (Holmes *et al*, 2013). However, beyond the knowledge that aggregates transit through vesicles to enter cells, the cellular factors involved in this process are unknown. To shed light on this process, we conducted a screen with a membrane trafficking siRNA library. We confirmed that, in our cellular system, aggregates penetrated inside cells using high resolution confocal microscopy (movie EV1). Aggregate uptake was quantified by high-throughput and automated image analysis in human 293T cells using high-content microscopy, following reverse-transfection with pools of 4 siRNAs per gene prior to Dylight-650-labeled mutant SOD1 aggregates inoculation (Fig. 1A, Fig. EV1A and B and Methods). The technical reproducibility of four independent screens allowed us to combine the different dataset and hits were ranked according to the combined *Z*-score of all experimental repeats (Fig. EV2A and B and Fig. 1B). The top hit of the screen was PICALM (Fig. EV2B), a clathrin-coated-pit adaptor protein homologous to AP180, which we previously reported (Münch *et al*, 2011). Knockdown of PICALM increased SOD1 aggregate uptake indirectly by the following mechanism: it decreases clathrin-mediated endocytosis, to which cells compensate by increasing other endocytic routes, in turn resulting in increasing SOD1 aggregate uptake (Münch *et al*, 2011). The presence of PICALM in the screen provided confidence that the siRNA screen identified relevant hits. This also confirms our previous findings showing that clathrin-mediated endocytosis does not mediate SOD1 aggregate entry (Münch *et al*, 2011).

We next performed a secondary validation screen for the top 15 genes (Z-score > 3.8 or < -3.8) using stringent validation criteria previously used in an siRNA screen for HIV restriction factors (Liu *et al*, 2011) (Fig. EV2C and D). The 9 out of 15 genes passed the secondary screen. The hits were next tested in an orthogonal experimental setup, measuring aggregate uptake by flow cytometry, as described (Münch *et al*, 2011). First, we confirmed that the method enabled the detection of internalized aggregates (Fig. EV3), as previously reported (Münch *et al*, 2011). This second validation yielded 5 genes: cofilin-1, RHO-associated protein kinase 1 (ROCK1), the Ras-related proteins RAB5C, RAB10 and sorting nexin-1 (SNX1) (Fig. EV2C and D and Fig. 1C). We also confirmed that individual siRNA against CFL1, ROCK1, RAB5C, RAB10 as well as sorting nexin-1 (SNX1) efficiently reduced their respective mRNA levels (Fig. EV4). Having performed the primary screen and validation in 293T cells, we next tested the different modifiers in a neuronal cell line. The relevance of the five validated modifiers of SOD1 aggregate uptake was confirmed in the neuronal cell line SK-N-AS (Fig. 1D and Fig. EV5). We next performed additional controls to assess the selectivity of the hits identified. RAB5C is one of three isoforms of RAB5 and the siRNA screen selectively identified RAB5C as a modifier of SOD1 aggregate entry. We confirmed that this effect was indeed specific because knockdown of RAB5A or RAB5B did

not affect SOD1 aggregate uptake (Fig. EV6). These results validate the screening method and identify modifiers of SOD1 aggregate uptake.

Signaling through RHO, ROCK1, LIMK1 to cofilin-1 regulates SOD1 aggregate entry into cells

We found remarkable that two of the top five hits, ROCK1 and cofilin-1 belong to the same pathway. This provided strong evidence to suggest that the ROCK1-cofilin-1 pathway was important for aggregate uptake and to examine this pathway in depth. Cofilin-1 is an actin de-polymerization factor, a crucial regulator of actin dynamics (Lappalainen & Drubin, 1997) whose activity is restricted by phosphorylation by the LIM-kinase 1(LIMK1) (Mizuno *et al*, 1998; Maekawa *et al*, 1999). LIMK1 is itself regulated by the kinases ROCK1 and RHO (Maekawa *et al*, 1999) (Fig. 2A). Indeed, knock-down of ROCK1 decreased cofilin-1 phosphorylation (Fig. 2B and C). Likewise, the RHO inhibitor CT04 as well as the ROCK1 inhibitor Y27632 also decreased cofilin-1 phosphorylation (Fig. 2D-G). Conversely, overexpression of LIMK1 increased cofilin-1 phosphorylation (Fig. 2H and I). Having found that cofilin-1 siRNA decreased aggregate uptake whilst ROCK1 siRNA increased aggregate uptake (Fig. 1C and D), we next tested whether the diverse manipulations of the RHO to cofilin-1 signaling pathway described above affected aggregate uptake. We found that both the RHO inhibitor CT04 and the ROCK inhibitor Y27632 increased mutant SOD1 aggregate uptake (Fig. 2J and K). Conversely, overexpression of LIMK1 decreased aggregate uptake (Fig. 2L). These findings were validated in primary neurons where both RHO inhibition and ROCK inhibition increased mutant SOD1 aggregate uptake (Fig. 2M). These results provide multiple independent lines of evidence establishing that a decrease in RHO signaling increases cofilin-1 activity to increase aggregate entry.

Remodeling of the cortical actin barrier through cofilin-1 is required for SOD1 aggregate entry

To gain insights into the underlying mechanism by which cofilin-1 facilitates aggregate entry, we next examined actin dynamics, knowing that cofilin-1 is an actin depolymerizing factor. As expected (Mizuno, 2013), knock-down of cofilin-1 increased cortical actin, as revealed by phalloidin staining (Fig. 3A) a finding confirmed by biochemical fractionation of F-actin and G-actin (Fig. 3B and C). ROCK1 knock-down had the opposite effect on the F/G actin ratio (Fig. 3D and E) and aggregate uptake (Fig. 1C and D). Both the RHO inhibitor CT04 and the ROCK inhibitor Y27632, which increased mutant SOD1 aggregate uptake (Fig. 2J and K) and decreased cofilin-1 phosphorylation (Fig. 2D-G), decreased F/G actin ratio (Fig. 3F and G). Jasplakinolide (Holzinger, 2009), which promotes actin polymerization also reduced SOD1 aggregate uptake (Fig. 3H and I). These results suggest that cortical actin forms a restriction barrier to aggregate entry and inhibition of RHO signaling promotes reorganization of cortical actin to enable aggregate entry (Fig. 3J).

To further investigate how alteration of cofilin-1 regulates aggregate entry, we monitored cofilin-1 activity following aggregate inoculation. Because cofilin-1 is regulated by phosphorylation (Mizuno *et al*, 1998; Maekawa *et al*, 1999) we examined the levels of phospho-cofilin-1 by immunoblots at different time after aggregate inoculation. The total cofilin-1 protein levels did not measurably vary following aggregate inoculation (Fig. 4A).

However, phosphorylation of cofilin-1 decreased between 10 and 60 minutes following aggregate inoculation (Fig. 4A and B). Interestingly, following this initial decrease, phospho-cofilin-1 levels then increased 1 hour after aggregate inoculation. This indicates that aggregates elicited a transient decrease in cofilin-1 phosphorylation, further supporting the notion that aggregates exploit cofilin-1 to enter cells and remodel actin. The increased cofilin-1 phosphorylation following an initial decrease indicates the existence of a negative feedback response where cells react to the initial alteration by increasing cofilin-1 phosphorylation. Indeed, cofilin-1 dephosphorylation leads to actin disassembly, which in turn increases cofilin-1 phosphorylation (Nagata-Ohashi *et al*, 2004; Soosairajah *et al*, 2005; Liu *et al*, 2015). Importantly, the changes in cofilin-1 phosphorylation were not observed when cells were inoculated with dextran (Mr ~ 10,000) instead of SOD1 aggregates (Fig. 4C and D), establishing the selective nature of the changes induced by SOD1 aggregates (Fig. 4A and B). The bi-phasic nature of the changes in cofilin-1 phosphorylation observed here (Fig. 4A and B) is also a hallmark of HIV-1 infection (Yoder *et al*, 2008). The role of cofilin-1 in aggregate entry identified here reveals a mechanistic analogy between SOD1 aggregate entry and the entry of some viruses, which also exploits cofilin-1 to remodel actin and enter cells (Yoder *et al*, 2008; Xiang *et al*, 2012; Zheng *et al*, 2013).

Cofilin-1 phosphorylation increases over time in SOD1^{G93A} transgenic mice

To examine the possible pathological relevance of our findings, we monitored cofilin-1 activity in transgenic mice expressing the human ALS-causing mutant SOD1^{G93A} (Gurney *et al*, 1994). The transgenic SOD1^{G93A} mice develop a motor neuron disease that closely resembles human ALS with progressive deposition of mutant SOD1 (Johnston *et al*, 2000; Wang *et al*, 2009) and progressive motor neuron loss leading to motor deficits. As previous noted in different transgenic SOD1 lines (Johnston *et al*, 2000; Wang *et al*, 2009), insoluble SOD1^{G93A} accumulated in the spinal cord of SOD1^{G93A} transgenic mice, as the disease progressed (Fig. 5A). Coincidentally, phosphorylation of cofilin-1 increased over time in the SOD1^{G93A} transgenic mice, whilst the total levels of cofilin-1 were not measurably altered (Fig. 5A and B). This is analogous to what has been observed in cells, where an increase in cofilin-1 phosphorylation follows an initial transient decrease (Fig. 4A and B). Whilst the bi-phasic nature of the changes in cofilin-1 phosphorylation cannot be captured in a mouse model, the alteration of cofilin-1 activity in vivo demonstrates the pathophysiological importance of cofilin-1 in this disease model. The changes in cofilin-1 phosphorylation observed in the spinal cord of SOD1 transgenic mice were associated with an increased F/G-actin ratio (Fig. 5C and D). These alterations were specific to the spinal cord, the affected tissue in the SOD1^{G93A} mice because no such changes were observed in the brains of the transgenic mice (Fig. 5E and F). These results argue that cofilin-1 signaling is altered in SOD1^{G93A} mice.

Relevance of modifiers of SOD1 aggregate uptake to diverse protein aggregates

The diverse misfolded proteins associated with neurodegenerative diseases spread just like prions (Jucker & Walker, 2011) suggesting that some of the mechanisms underlying such properties may be shared. Having identified here a set of host factors modulating entry of SOD1 aggregates in cells and realizing that the actin barrier is also important in restricting viral entry, we next investigated whether the validated genes identified in the screen

performed with SOD1 aggregates were relevant to other disease-related protein aggregates. Aggregates made of α-synuclein, the major component of deposits in Parkinson's disease, also spread from cell to cell (Danzer *et al*, 2007; Desplats *et al*, 2009). Recombinant α-synuclein was produced as previously described (Murray *et al*, 2003), aggregated, labelled with Dylight-650, and sonicated before being inoculated to cells, as previously reported (Danzer *et al*, 2007; Desplats *et al*, 2009). We next investigated whether the 5 validated genes identified in the SOD1 screen also modulated entry of α-synuclein fibrils inside cells. As observed for SOD1 aggregates, we found that siRNA against cofilin-1, RAB5C and RAB10 decreased aggregate entry whilst siRNA targeted at ROCK1 and SNX1 increased entry of α-synuclein aggregates (Figure 6A). Pharmacological inhibition of RHO also increased α-synuclein fibrils entry (Figure 6B), confirming that signaling upstream of cofilin-1 is required to modify aggregate entry. Conversely, Jasplakinolide, which promotes actin polymerization reduced aggregate entry (Figure 6C). This demonstrates that the RHO-Cofilin-1 signaling pathway leading to changes in actin dynamics modulates entry of two unrelated protein aggregates, $SOD1^{G93A}$ and α-synuclein.

To further explore the possible general relevance of our findings to different protein aggregates, we next investigated the effect of the modifiers identified in the SOD1 screen on uptake of Dylight-labelled recombinant Tau aggregates prepared as described (Falcon *et al*, 2015). With the exception of RAB10, all the modifiers of SOD1 and α-synuclein also modified entry of Tau aggregates (Figure 6D). Importantly, as for SOD1 and α-synuclein aggregates, inhibition of RHO increased Tau aggregates entry (Figure 6E), whilst Jasplakinolide reduced aggregate entry (Figure 6F). Thus, diverse protein aggregates exploit the RHO-ROCK1-cofilin-1 signaling pathway to overcome the actin barrier and invade cells, just like viruses do (Fig. 6G).

Discussion

Using a focused siRNA screen, we have discovered that SOD1 aggregates exploit the actin depolymerizing factor cofilin-1, a crucial regulator of actin dynamics, to remodel cortical actin and enter cells. Through a combination of approaches, we show that upstream of cofilin-1, signaling through RHO, ROCK1 and LIMK1 restricts cofilin-1 activity to stabilize cortical actin filaments, which act as a barrier to prevent aggregate entry. This work provides novel mechanistic insights in SOD1 aggregate entry, a process which has been poorly characterized so far, and identifies host factors modulating aggregate entry.

Recently, the realm of prions has expanded. There is now abundant literature showing that the diverse proteins associated with neurodegenerative diseases share the defining features of prions (Jucker & Walker, 2011; Brundin *et al*, 2010; Frost & Diamond, 2010; Goedert *et al*, 2010; Munch & Bertolotti, 2012). The mechanism underlying the prion-like spread of disease-causing proteins is unknown, particularly for aggregates that spread from cell to cell. Here we focused on identifying one of the earliest events in this process, the internalization of aggregates, and reveal host cell factors mediating aggregate entry. Importantly, we show that aggregates made of the diverse disease-causing proteins, mutant SOD1, α-synuclein or Tau, exploit the RHO to cofilin-1 signaling pathway to weaken cortical actin, the first

intracellular barrier, and enter cells. This defines yet another common molecular feature to diverse neurodegenerative diseases.

Previously, we reported that mutant SOD1 enter cells using macropinocytosis (Münch *et al*, 2011), a finding recapitulated by others (Yerbury, 2016). Tau aggregates were also subsequently found to use macropinocytosis to enter cells in different studies (Holmes *et al*, 2013; Sanders *et al*, 2014; Falcon *et al*, 2015). However, further progress has been hindered by the fact that macropinocytosis is not well defined and due to the lack of specific agents to manipulate this process. Incidentally, the identification of cellular factors, cofilin-1 and its regulators, as modifiers of aggregate entry provides a framework for future investigations of a possible role of cofilin in macropinocytosis.

Our results reveal a pathway mediating aggregate entry. Through a combination of diverse pharmacological manipulations or knock-down of RHO, ROCK1 or LIMK1, we found that the dynamics of cofilin-1 activity and actin polymerization is an important control of aggregate entry. This demonstrates the importance of cortical actin in forming a barrier to aggregate entry. However, it is noteworthy that none of the manipulations completely prevent aggregate entry, suggesting that cells adapt to the manipulations or that some alternative entry routes might be utilized, when one is compromised. Interestingly, some viruses can use multiple routes to enter cells (Cossart & Helenius, 2014). The changes in cofilin-1 activity during aggregate entry is bi-phasic, implying that actin ought to play a dual role in this process: at early stage of aggregate entry, actin depolymerisation is required in order to weaken cortical actin which acts as a barrier to aggregates. This change is transient, with a rapid increase in cofilin-1 phosphorylation following the initial decrease, probably due to a negative feedback loop. Indeed, cofilin-1 dephosphorylation leads to actin disassembly, which in turn increases cofilin-1 phosphorylation (Nagata-Ohashi *et al*, 2004; Soosairajah *et al*, 2005; Liu *et al*, 2015). Although the dynamic of cofilin-1 signaling cannot be captured *in vivo,* we find remarkable that cofilin-1 phosphorylation dramatically increases with age in $SOD1^{G93A}$ spinal cord. This increased cofilin-1 phosphorylation leads to its inactivation and results in an increase in filamentous actin. This establishes that cofilin-1 and actin dynamics are altered in a mouse model of ALS. Considering the broad importance of actin function, such an alteration in actin dynamics ought to be deleterious. Further confirming the pathological relevance of these findings, these alterations were not widespread but restricted to the degenerating spinal cord. Thus, alteration of cofilin-1 signaling and actin dynamics appears tightly correlated to neurodegeneration. Importantly, as we have found here in SOD1-ALS mice, increased cofilin-1 phosphorylation was observed in post-mortem samples from ALS patients (Sivadasan *et al*, 2016). In addition, genetic links between ALS and alteration of actin dynamics also exist with mutations in the gene encoding the actin-binding protein profilin 1, a protein with dual function on actin dynamics, causing familial ALS (Wu *et al*, 2012). The most common genetic cause of ALS and frontotemporal dementia consists in an aberrant hexanucleotide repeat expansions in C9orf72 (Guerreiro *et al*, 2015). These repeats are translated in di-peptide repeat proteins which also spread like prions (Westergard *et al*, 2016). Intriguingly, C9orf72 was found to interact with cofilin-1 and to increase cofilin-1 phosphorylation through LIMK1/2 (Sivadasan *et al*, 2016). Our findings provide a mechanistic starting point to evaluate the interplay between cofilin-1, actin dynamics and the spread of aggregates.

It is noteworthy that some viruses such as Human Immunodeficiency Virus, Herpes Simplex Virus 1 (HSV1) and rotavirus, also exploit cofilin-1 for cell entry (Yoder *et al*, 2008; Zheng *et al*, 2013; Berkova *et al*, 2007). Like SOD1 aggregates, both HIV1 and HSV1 infection cause bi-phasic change in cofilin-1 activity to promote actin dynamics and enter cells (Yoder *et al*, 2008; Xiang *et al*, 2012; Zheng *et al*, 2013). It is remarkable that the strategy revealed here and used by different protein aggregates to penetrate inside cells shares similar components to those employed by some viruses. This reinforces the notion that protein aggregates share some of the properties of infectious agents.

Materials and methods

Protein purification, labelling and aggregation

SOD1—Recombinant human H46R mutant SOD1 protein was purified from Sf9 cells as described previously (Münch *et al*, 2011). Purified SOD1 was crosslinked with Dylight650 N-hydroxysuccinimide (NHS) Ester (Thermo Fisher Scientific) according to the manufacturer's instructions.

To generate aggregates, labelled and unlabelled SOD1 were mixed (5 and 10 μM respectively) with 20% 2, 2, 2 - trifluoroethanol (TFE, Sigma-Alrich) and MES (0.5 M, pH 6.3) for 24 hours. The aggregates were purified by centrifugation at 20,000g for 10 minutes at room temperature. Supernatant containing free dye and soluble protein was removed. The pellet was re-suspended in Tris-NaCl buffer (10 mM Tris-HCL pH 8, 100 mM NaCl), and briefly sonicated before use (3 minutes, 1s on/off). SOD1-Dylight650 aggregates were used as a final concentration of 0.8 μM (monomer equivalent).

α-synuclein—Recombinant human α-synuclein was cloned into pRK172 vector and transformed in BL21 competent *E. coli* cells (NEB). Protein expression was induced by 0.1 mM IPTG for 4 hours at 37°C in TB broth. The pellet of 1L culture was resuspended in 50 ml of lysis buffer supplemented with protease inhibitors (50 mM Tris-HCl pH7.4, 2 mM EDTA, 5 mM MgSO4, 5 mM DTT, 0.2 mM PMSF, Protease inhibitor and 20 mM NaCl). Cells were sonicated and spun at 30,000 rpm in a TLA45 rotor (Beckman) for 30 minutes. Filtered supernatant containing α-synuclein was precipitated by 30% ammonium sulfate and centrifuged at 30,000 rpm in a TLA45 rotor (Beckman) for 30 minutes. The pellet was resuspended in lysis buffer and loaded on a 5 ml HiTrap Q HP anion-exchange column (GE Healthcare). Elution was performed using a 0-1 M NaCl gradient. α-synuclein eluted at around 150 mM NaCl. Fractions containing α-synuclein were pooled and further purified by size exclusion a HiLoad 16/600 Superdex 200 PG column (GE Healthcare) in a buffer containing 50 mM Tris-HCl pH7.4, 2 mM EDTA, 5 mM MgSO4, 5 mM DTT and 20 mM NaCl. Fractions containing α-synuclein (76-90 ml) were pooled and concentrated. α-synuclein aggregation was induced by incubating protein at 37°C with 450 rpm shaking for 5 days. Protein fibrillization was confirmed using the thioflavin T (T3516, Sigma-Aldrich) fluorescence assay. Protein aggregates were labelled with Dylight-650 (Thermo Fisher Scientific) according to manufacturer's instructions. Aggregates were sonicated (3 minutes, 1s on/off) before use. α-synuclein-Dylight-650 aggregates were used at a final concentration of 0.1 μM (monomer equivalent).

Tau—Recombinant Tau-441(2N4R) isoform protein was purchased from AnaSpec (AS-55556-100, AnaSpec EGT Corporate Headquarters). In vitro fibrillization of full-length Tau (2N4R) was prepared by mixing with 300 mM recombinant Tau, 50 mM low molecular weight heparin and 2 mM DTT in 100 mM sodium acetate buffer under constant orbital agitation (1,000 rpm) at 37°C for 3 days (Falcon *et al*, 2015). Aggregates were labelled with Dylight-650 (Thermo Fisher Scientific) according to manufacturer's instructions and were sonicated (3 minutes, 1s on/off) before being inoculated into cells. Dylight-650-tau aggregates were inoculated at a final concentration of 0.06 μM (monomer equivalent).

Three dimension (3D) images process—High resolution images of aggregates taken up by cells were obtained on a Leica SP8 confocal microscope (Leica Microsystem Ltd.). Images were obtained using a HC PL APO CS2 63X 1.4 NA objective. Multiple image planes were obtained, sampled at a spacing of 60nm by 60nm (lateral direction) and 300nm (axial direction). Other Leica SP8 settings were Zoom 3, 5x line average, 600Hz scan speed, 1024 x 1024 array size. The pinhole was set equivalent to 1 Airy at 580 nm for all channels. The microscope spectral detection windows were set as follows. H33342: excitation 405nm, detection 410nm to 475nm; CellMask Green: excitation 514nm, detection 518nm to 593nm; and Dylight650-SOD1: excitation 633nm, detection 639nm to747nm. The green and far red signals were imaged on separate scans of the sample to minimise bleedthrough. Image stacks were segmented in three dimensions using Imaris Software (BITplane AG).

siRNA screen

siRNA libraries and plates preparation—Two SMARTpool siRNA libraries, containing 4 unique ON-TARGETplus siRNA duplexes targeting total 224 genes, were used in the screen. Human Membrane Trafficking library (GE Healthcare, 140 genes) was used in plate 1 and plate 2. A custom membrane trafficking (84 genes) was used in plate 3 and 4. Non-targeting siRNA were used as controls (column 1 and 12) as well as mock transfections.

SMARTpool siRNA library (GE healthcare) were aliquoted into Poly-L-lysine (Sigma-Aldrich) coated CellCarrier 96 microplates (PerkinElmer) as stock plates and stored at -20°C. siRNA reverse transfection in plates was conducted by using DharmaFECT1 (GE healthcare) transfection reagent. After 72 hours of transfection, 0.8 μM Dylight-650 labelled SOD1 in fresh medium, was passed through a 0.45 μm filter and incubated in each well for 16 hours (overnight).

Cells were washed by PBS and incubated with CellMask green plasma membrane stain (1:1000; Thermo Fisher Scientific) and H33342 (1:10,000; Thermo Fisher Scientific) in PBS for 10 min. Cell plates were then fixed by 4% PFA for 15 min at room temperature before imaging.

Image acquisition and processing—96 well plates were imaged using a Nikon High content analysis system under the control of NIS Elements JOBS software (Nikon UK Ltd). Images were obtained using a 20X 0.75 NA Plan Apo objective. A cropped camera array field corresponding to 630 x 630 μm in object space was used. Nine images were obtained in a regular 3 by 3 grid, spaced 1 mm apart, centred in each well. At each position, a three-

channel fluorescence image was taken as follows. H33342 (blue): emission 435nm to 485nm, typical exposure time 40 msec; CellMask green stain: emission 500nm to 550nm, typical exposure time 200 msec; Dylight650-SOD1 (far red): emission 663nm to 738nm, typical exposure time 500 msec. Whilst fixed exposure values were used across each set of plates, some adjustments to the exposure time were made between replicates. At each position the system first performed an auto focus operation using the CellMask green signal.

Images were analyzed using the 'general analysis' tool in NIS-Elements-HC software (Nikon UK Ltd). Individual nuclei were segmented to give a count of the number of cells per field. The CellMask green image was used to create a binary mask defining the area of the cells. Aggregates were identified using a spot detection tool. The total number of spots lying within the cell area binary mask, per field was counted.

Secondary screen—The top 15 genes from the primary screen were applied to a secondary screen by set of 4 single siRNAs knockdown. Transfections of 4 single siRNA per gene were conducted as before in a 96 well plates. The Z score threshold of 1.5 was applied in the secondary screen. The criterion is that at least 2 out of 4 siRNA must be hits to be considered 'on-target'. Any gene containing contradictory results from the 4 single siRNAs was not taken into further validation. Genes which passed the secondary screen were used for further validation. Dharmacon ON-TARGETplus Non-targeting siRNA (D-001810-01-05) was used as a negative control. The sequences of the validated siRNA are: CCUCUAUGAUGCAACCUAU for CFL1; GAACAAGAUCUGUCAAUUU for RAB5C; CUACAAGUGUUGCUAGUUU for ROCK1; CACGUUAGCUGAAGAUAUC for RAB10; GGAAAGAGCUAGCGCUGAA for SNX1. RAB5A and RAB5B gene knockdown were conducted by siRNA SMARTpool (GE Dharmacon L-004009 and L-004010 independently).

Mammalian cell culture—HEK293T cells were maintained in DMEM medium (11960044, ThermoFisher Scientific) supplemented with L-glutamine-penicillin-streptomycin solution (G6784; Sigma-Aldrich) and 10% fetal bovine serum (FBS, 10270, ThermoFisher Scientific). SK-N-AS cells (ATCC, Cat#CRL2137) were cultured in DMEM medium supplemented with 1% MEM Non-Essential Amino Acids (11140050, ThermoFisher Scientific), L-glutamine-penicillin-streptomycin solution and 10% FBS.

Cells were routinely tested for mycoplasma contaminations (GATC Biotech).

Primary neuron culture—C57 JAX mice were obtained from the Jackson Laboratories. Primary cortical neurons were prepared from E15.5 pups and cultured in Neurobasal media supplemented with B-27 (Invitrogen) supplemented with L-glutamine-penicillin-streptomycin solution (G6784; Sigma-Aldrich) on tissue culture plates coated with Poly-L-lysine (Sigma-Aldrich). The neurons were maintained by changing medium every 3-4 days.

Expression of plasmids and siRNAs—Human LIMK1 cDNA in entry gateway cloning vector was obtained from GE Healthcare (Cat#OHS5894-202502218) and recombined with pTGSH-HA vector (Dualsystems Biotech AG) to produce the expression construct pTGSH-LIMK1 with a C-terminal hemagglutinin-Strep tag. All plasmids were

verified by sequencing. For transient transfection, cells were plated in 24 well plates and constructs were transfected with FUGENE HD transfection reagent (Promega UK) for 48 hours.

siRNA were transfected with Lipofectamine RNAiMAX (Thermo Fisher Scientific) in SK-N-AS cells, plated in complete medium in 24 well plates at a concentration of 10^5 cells/ml one day before the transfection. For the screen, siRNA were reverse transfected into HEK293T cells. Briefly, DharmaFECT1 was diluted in OptiMEM (Thermo fisher scientific) and added to wells with siRNA to make the RNAi-Dharma complex. HEK293T cells in complete growth medium (3×10^4 cells/ml) were plated in each well to give a final concentration of 50 nM of siRNA. Cells were collected 48 hours or 72 hours after transfection.

Cell treatments—RHO inhibitor CT04 (1 μg/ml; Cytoskeleton, Inc.), ROCK inhibitor Y27632 (10 μM; Tocris) or Jasplakinolide (25nM; Santa Cruz) were applied to SK-N-AS in serum free medium for 16 h or primary neuron for 1 hour.

Alexa488-Dextran (Mr ~ 10,000, Thermo Fisher Scientific) was dissolved in DMSO as 10 mg/ml stock. SK-N-AS cells were replaced by 0.5% serum medium for 16 h before 3.2 μM (monomer equivalent) SOD1 aggregates (prepared as before) or 800μg/ml Dextran inoculation for the indicated time.

Quantitative RT-PCR—Knockdown of genes was confirmed by quantitative RT-PCR (qPCR) 48 hours after siRNA transfections in 96 well plates. RNA was extracted with RNeasy mini kit (Qiagen) according to the manufacturer's instruction. 500 ng RNA was reverse transcribed to cDNA with the iScript cDNA synthesis Kit (Biorad) according to the manufacturer's instruction. qRT-PCR gene amplification was conducted with CYBR Select Master Mix (Applied Biosystems) in Corbett Research Rotor-Gene real-time PCR machine version 6000 (Thermo Fisher Scientific). Expression of each gene was normalized to the housekeeping gene *gapdh* and expressed as fold change ($2^{\Delta\Delta CT}$). qPCR primers: CFL1 (F: GTGCCCTCTCCTTTTCGTTT; R: TTGAACACCTTGATGACACCAT); RAB5C (F:CCGCTTTGTCAAGGGACAGTT; R:AGGCTGTGATACCGCTCCT); ROCK1 (F:GATCCCAAATCGGAAGTGAA;; R:CAAATCATATACCAAAGCATCCAA); RAB10 (F:TTCGGATGATGCCTTCAATA; R:AGGAGGTTGTGATGGTGTGA); SNX1 (F:CATGTTACAGGACCCTGACG; R:GACCAGCACCACTCAATGTC); GAPDH (F: ACCACAGTCCATGCCATCAC; R: TCCACCACCCTGTTGCTGTA).

Flow cytometry—0.8 μM Dylight650-SOD1^{H46R} (0.1 μM Dylight650-α-synuclein or 0.06 μM Dylight650-tau) aggregates were inoculated in cells for the times indicated. The excessive aggregates were removed by washing with PBS. Cells were digested with 0.25% trypsin to digest the extracellular aggregates and to produce a single-cell suspension. Fluorescence intensity of was measured by flow cytometry on 10,000 cells per sample on a LSRFortessaTM (BD Biosciences). FlowJo (v10) (FlowJo LLC) was applied for fluorescence intensity quantification. The median fluorescence intensity of each sample was normalised to control.

Immunoblot—Cells or mouse tissue was lysed with RIPA buffer (Cell Signaling Technology) plus Protease inhibitor and PhosStop (Sigma-Aldrich). Cell lysates were sonicated and quantified with the BCA assay kit (Pierce BCA Protein Assay Kit, Thermo Fisher Scientific). Samples were boiled with Laemmli Buffer at 95°C for 5 minutes and loaded onto Bolt 4-12% Bis-Tris plus gel (Thermo Fisher Scientific) in MES buffer. Gels were transferred to nitrocellulose membranes (Thermo Fisher Scientific). Membranes were incubated with antibodies as following: anti-CFL1 (1:10,000; Abcam, ab42824); anti-pCFL1 (1:1,000; Cell Signaling Technology, 77G2); anti-ROCK1 (1:2,000; Abcam, ab45171); anti-GAPDH (1:2,000; Millipore); anti-actin (1:1,000; Abcam, ab3280) and anti- human SOD1, clone C4F6 (1:1000; Medimabs, Cat#MM-0070-2-P). Horseradish peroxidase conjugated anti-mouse or anti-rabbit antibody was used as secondary antibody (Promega). Membranes were revealed with ECL Prime (GE Healthcare) and ChemiDoc Touch (Biorad).

F-actin and G-actin separation and F-actin/G-actin ratio determination—F/G actin was fractionated with G-actin/F-actin in vivo assay kit (Cytoskeleton, Inc) according to the manufacturer's instruction. Briefly, the cell or mouse tissue was lysed with LAS2 buffer at 37°C for 10 mins. Cell debris were removed by centrifugation at 2,000 rpm for 5 min. 100 μl of the supernatant was ultra-centrifuged (Beckman rotor TLA55) at 100,000 g for 1 hour at 37°C to separate the G-actin (supernatant) and F-actin (pellet). The pellet was lysed with 100 μl of F-actin depolymerisation buffer for 1 hour on ice. The samples were used for actin quantification by SDS-PAGE and immunoblot analysis.

SOD1 fractionation—Spinal cords from SOD1 mutant mice were homogenized (100mg/ml) in homogenization buffer (PBS containing 1 mM EDTA, 1 mM EGTA, and 10 mM TCEP, as well as 20 mM iodoacetamide plus complete protease inhibitor mixture (Sigma-Aldrich)). After centrifugation at 17,000g for 20 minutes, the supernatants were collected. Pellets were washed twice with the homogenization buffer, solubilized in Laemmli Buffer containing 100 mM of TCEP, sonicated for 5 mins and boiled at 95°C for 5 minutes. Protein samples from the soluble and insoluble extracts were separated and analyzed by SDS-PAGE and immunoblot analysis.

Immunofluorescence—Cells were fixed with 4% PFA in PBS for 8 min followed by permeabilization with 0.1% triton-X in PBS (PBST) and blocked with 5% normal goat serum (NGS)/PBS. Cells were stained with Alexa Fluor 594-Phalloidin (Invitrogen) (1:40 in 1% NGS/PBST) or anti-CFL1 antibody (1:10,000 in 1%NGS/PBST) at room temperature for 1 hour followed by Alexa Fluor 488 linked goat-anti-rabbit secondary antibody (Thermo Fisher Scientific) for another 1 hour, then mounted with Pro-Long gold antifade mountant (Thermo Fisher Scientific). Images were taken with the Zeiss 780 confocal microscope (Carl Zeiss Ltd.) using 63 x objective for *z* stacks. Images were typically 1,024 × 1,024 pixels. The stacks of *z*-section were recorded at 0.5-μm intervals to encompass the full width of each cell.

Mouse model—Mouse care and procedures were performed in compliance with the regulation on the use of Animals in Research (UK Animals Scientific Procedures Act of 1986 and the EU Directive 2010/63/EU) with local ethical approval.

SOD1 mice SOD1^{G93A} in C57BL/6J were used previously (Das *et al*, 2015) (Luh *et al*, 2017). The lumbar region of the spinal cord of SOD1^{G93A} and wild-type littermates as well as the whole brain were collected for analysis.

Quantification and statistical analysis—All data are presented as means ± SEM. Data were analyzed using One-Way ANOVA test followed by multiple comparison or unpaired t-test (two samples comparison) was applied using Prism 7.02 (GraphPad Software, La Jolla, CA). The level of significance was set at *p<0.05 as significantly different, and **p<0.01, ***p<0.001, ****p<0.0001 as highly significantly different. n.s. not significantly different, p≥0.05. The statistical method, sample number (n) and p values (t-test) are specified in each figure legends.

Statistical analysis in screen and ranking of genes—Screening data for each gene comprising location in the imaged well-plate array, cell count and number of fluorescent aggregates per cell were extracted for statistical analysis to detect any hit genes which, when knocked-down, give rise to significantly more or significantly fewer fluorescent aggregates than average.

Initially, the number of cells imaged in each sample was assessed to discount gene knock-downs that adversely affect cell viability. Accordingly, for each replicate experiment, a minimum accepted cell count was calculated as the value 1.5 standard deviations below the median count. Array locations with cell counts below this cut-off were excluded from further analysis.

Graphical representation of the spots per cell (SPC) data in a reconstructed color matrix form, corresponding to the siRNA well-plate (as used in Fig. EV3A), illustrated that there were systematic effects resulting from the samples' location in the experimental array. Accordingly, the first and last columns of the array were not used and the SPC data were normalized on a per-row basis.

The row based normalization involved scaling each row of SPC values so that the sum of adjusted SPC values is the same for all rows. The SPC data for each replicate were centered and scaled separately, by expressing them as primary *Z*-scores for each individual replicate. Subsequently these were then used to calculate a combined *Z*-score, considering all 4 replicates. The combined *Z*-scores were calculated from the distribution of the genes' mean primary score, i.e. the *Z*-normalized gene data from separate replicates was averaged and analysed to make a new score. All of the *Z*-scores were calculated using robust estimates for the centre and standard deviation of the respective distributions.

$$z = \frac{xi - median(xi)}{1.4826 \times medium(|xi - medium(xi)|}$$

The data were presented as a ranked gene list (see Fig. EV3B), according to the magnitude of the combined *Z*-score over all experimental repeats.

Europe PMC Funders Author Manuscripts

Extended Data

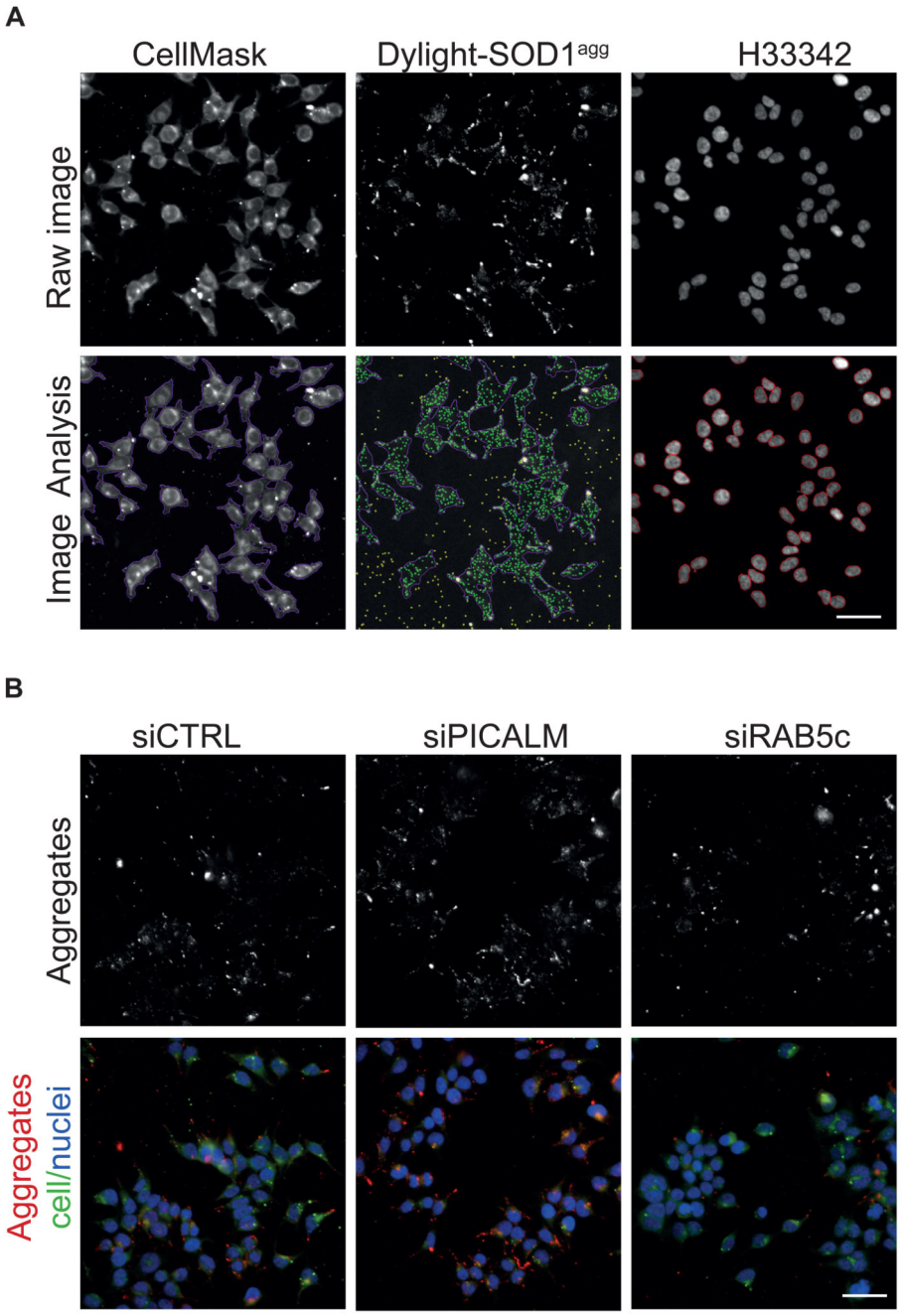

Figure EV1. Representative images of the siRNA screen.

A. Representative primary image samples extracted from the siRNA screen with the Nikon high content microscope (20x 0.75 NA objective). Upper row: Sub-region taken from a three-channel image of 293T cells treated for 16 hours with Dylight-650 labelled SOD1 aggregates. The sample was co-stained with H33342 (blue) to reveal nuclei and CellMask (green) to reveal plasma membrane. Lower row: results of image segmentation using the

Nikon NIS elements general analysis. Aggregates within cells are identified as green dots. CellMask reveals the outline of the plasma membrane artificially coloured as purple boundary. Yellow dots are rejected spots, being either aggregates outside of cells or containing saturated pixels. Red circle lines delineate the cell nuclei. Scale bar: 50 μm. **B.** High content images of 293T cells 3 days after transfection with control (CTRL) siRNA, PCALM siRNA or RAB5C siRNA and stained with H33342 (blue) to reveal nuclei, CellMask green plasma membrane stain (green). Cells were fixed and imaged after 16 hours flowing inoculation with Dylight-650labelled SOD1 aggregates (red). Scale bar: 50 μm.

Europe PMC Funders Author Manuscripts

Europe PMC Funders Author Manuscripts

A

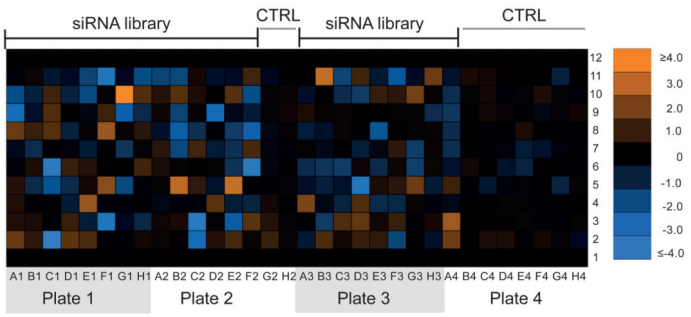

B

Gene	Z-score number of aggregates per cell: Screen 1	Screen 2	Screen 3	Screen 4	Screen 1-4	p-value	Cell count (Z-score)
PICALM	8.29	6.40	2.28	0.35	7.48	7.66E-14	0.10
ITSN2	2.39	3.17	2.79	4.87	5.70	1.20E-08	-0.54
RAB33A	2.22	1.97	3.65	4.94	5.51	3.52E-08	-0.54
PDCD6IP	3.14	3.86	1.86	3.69	5.42	6.11E-08	0.66
RAB9A	1.27	3.92	1.75	3.62	4.55	5.33E-06	-0.01
SNX1	2.54	3.01	1.85	2.74	4.37	1.25E-05	0.40
RAB1A	1.19	1.59	1.69	5.64	4.35	1.34E-05	-0.05
CFL1	-2.54	-2.90	-2.64	-1.98	-4.38	1.18E-05	0.54
CLTC	-0.80	-4.23	-2.45	-2.05	-4.15	3.34E-05	-0.30
MAP1LC3A	-2.83	-2.38	-3.25	-0.81	-4.04	5.32E-05	0.18
ARPC2	-1.48	-2.99	-3.49	-1.21	-4.00	6.36E-05	0.33
ROCK1	1.86	3.52	2.29	1.27	3.85	1.19E-04	-0.01
RAB10	-2.84	-2.78	-3.30	0.00	-3.89	1.01E-04	1.16
VAMP1	-2.88	-3.23	-1.78	-0.98	-3.87	1.10E-04	0.00
RAB5C	-2.12	-2.79	-3.10	-0.68	-3.79	1.48E-04	0.30

≥ 5.0
4.0
3.0
2.0
1.0
0.0
-1.0
-2.0
-3.0
-4.0
≤-5.0

C

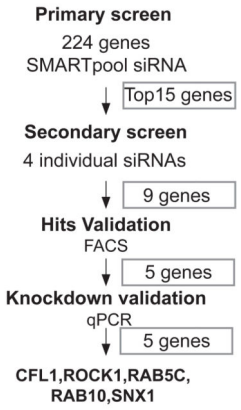

D

4/4	3/4	2/4	1/4	0/4
CLTC	CFL1	ROCK1	PDCD6IP	RAB1A
	RAB5C	RAB10	ARPC2	
	RAB9A	SNX1	MAP1LC3A	
	VAMP1	RAB33A	PICALM	
			ITSN2	

Figure EV2. Overview of siRNA screen procedure.

A. Upper panel: Color matrix representing the combined *Z*-score (protein aggregates per cell normalized to control) for each siRNA knockdown reconstructed at original well-plate grid locations.

B. Summary of siRNA screening results for the top 15 genes. Hits are ranked according to the absolute value of the combined *Z*-scores (screen1-4), normalized from average of experimental replicates (screen 1, screen 2, screen 3 and screen 4). *P* value is the estimated

probability of obtaining a value as combined *Z*-scores; the cell count corresponds to the mean of cell count *Z*-scores from four independent biological experiments.

C. Overview of the validation strategy of siRNA screen.

D. Number of individual siRNA (out of 4) per hit modifying SOD1 aggregate entry in secondary screen.

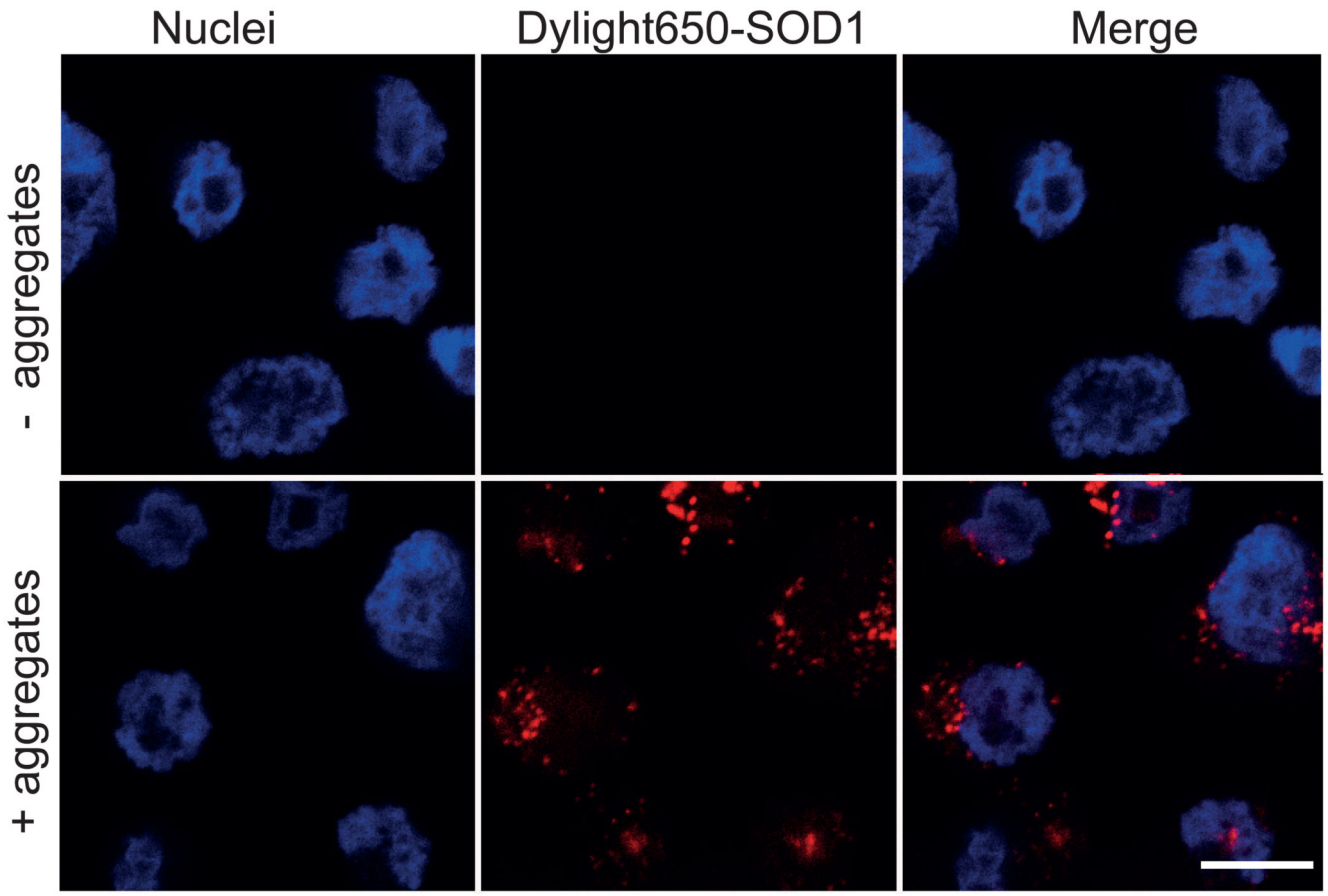

Figure EV3. Confocal images showing SOD1 aggregates are inside cells after trypsinization and prior to FACS analysis.

SK-N-AS cells were trypsinized and fixed after 2 hours following inoculation with Dylight--650 labelled SOD1 aggregates. Images were acquired with the Zeiss 710 confocal microscope (Carl Zeiss Ltd.) by 63X objective focusing on nuclei layer, to ensure that the images enable the visualization of the cellular content. Scale bar: 10 micrometers.

Europe PMC Funders Author Manuscripts

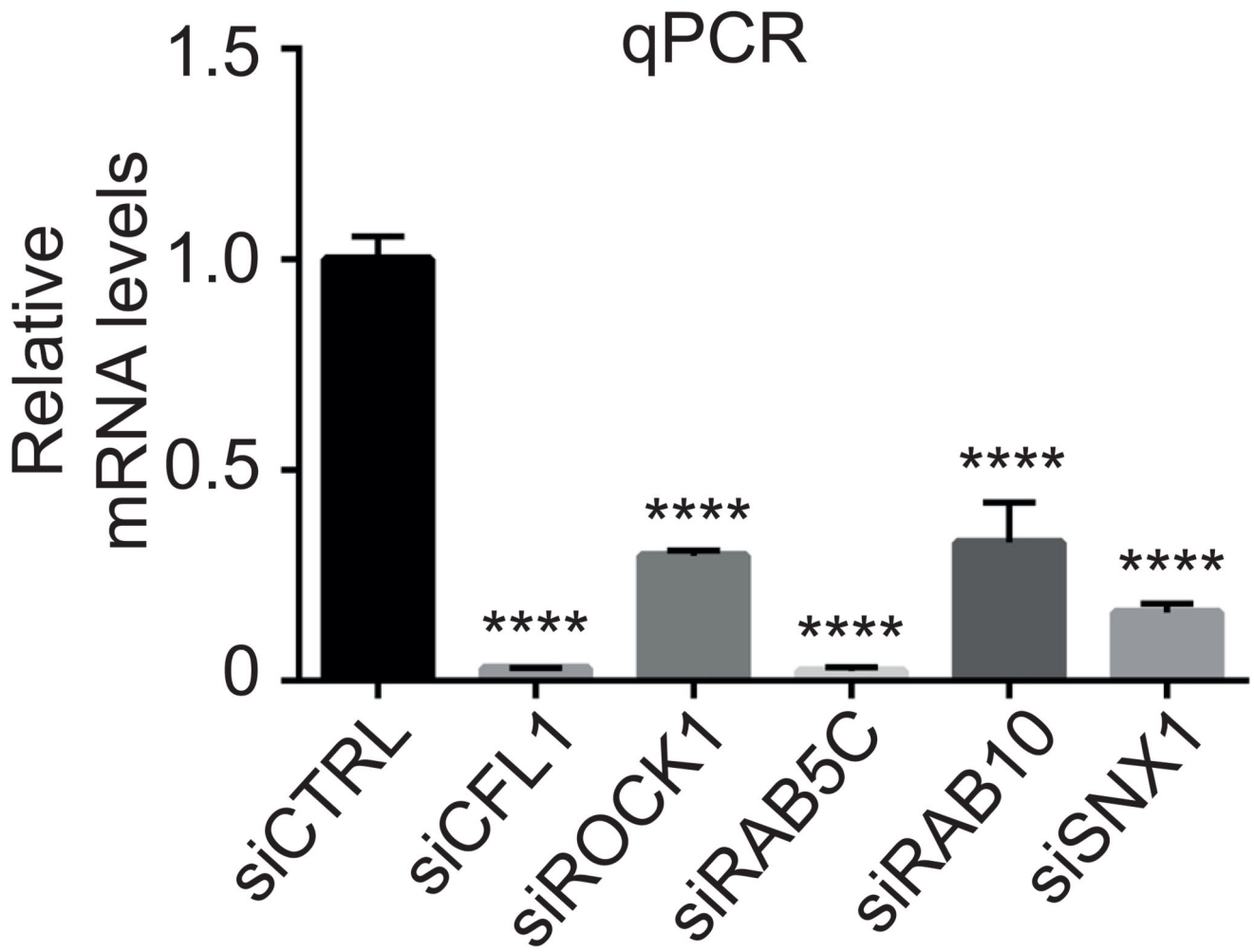

Figure EV4. siRNA knockdown of the five modifiers isolated in the screen.

mRNA levels measured by quantitative RT-PCR 2 days after transfection with the indicated siRNA. Data are means ± SEM. (n≥2). Ordinary one-way ANOVA followed by multiple comparisons. **** $P \leq 0.0001$.

Europe PMC Funders Author Manuscripts

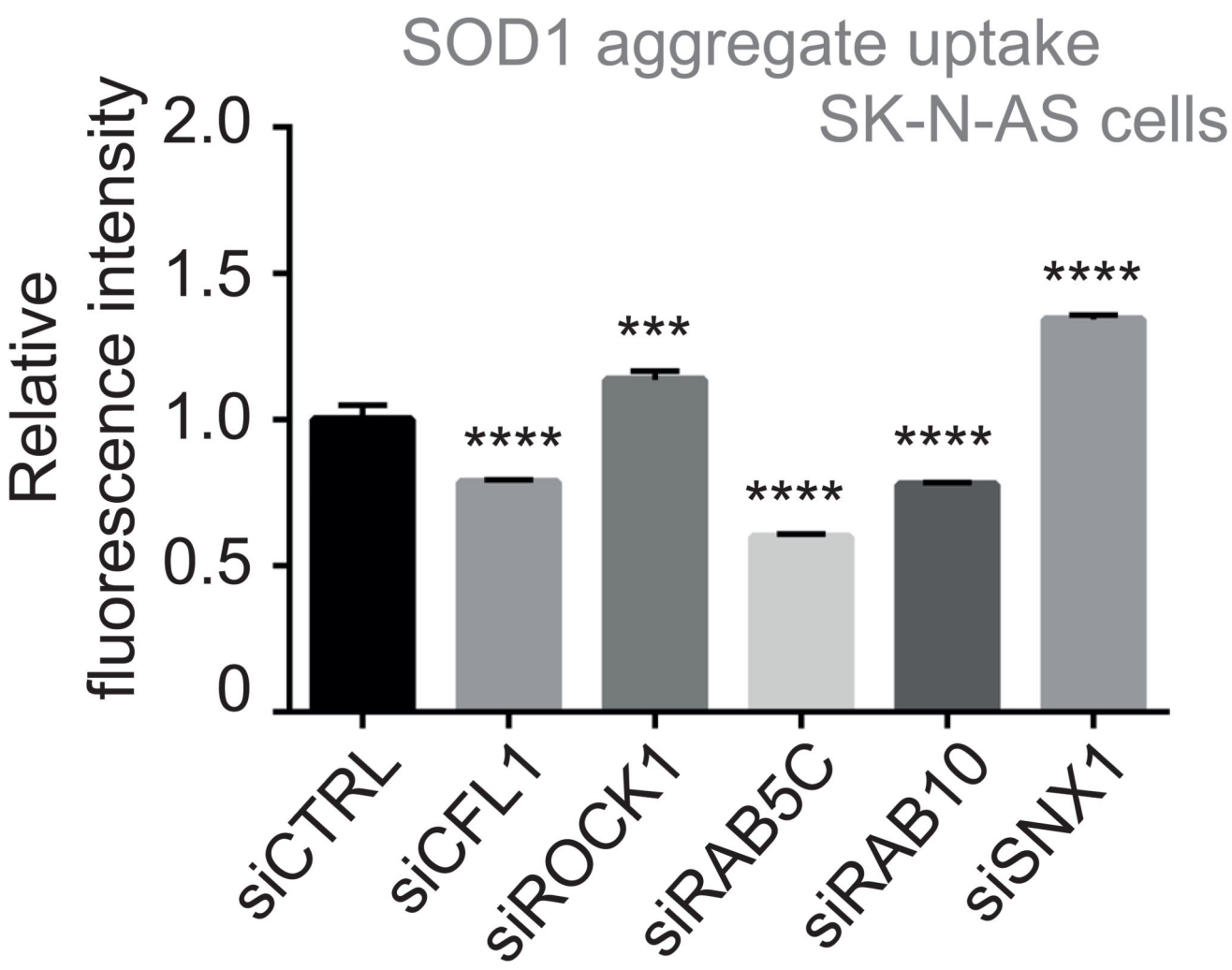

Figure EV5. Modifiers of SOD1 aggregate entry.

Flow cytometry analysis of SK-N-AS cells 16 hour after inoculation with 0.8 μM Dylight650-SOD1^{H46R} aggregates and 3 days after transfection with the indicated siRNA. Fluorescence intensity of was measured by flow cytometry on 10,000 cells per sample (n=3). Ordinary one-way ANOVA followed by multiple comparisons. *** $P \leq 0.001$, **** $P \leq 0.0001$.

Europe PMC Funders Author Manuscripts

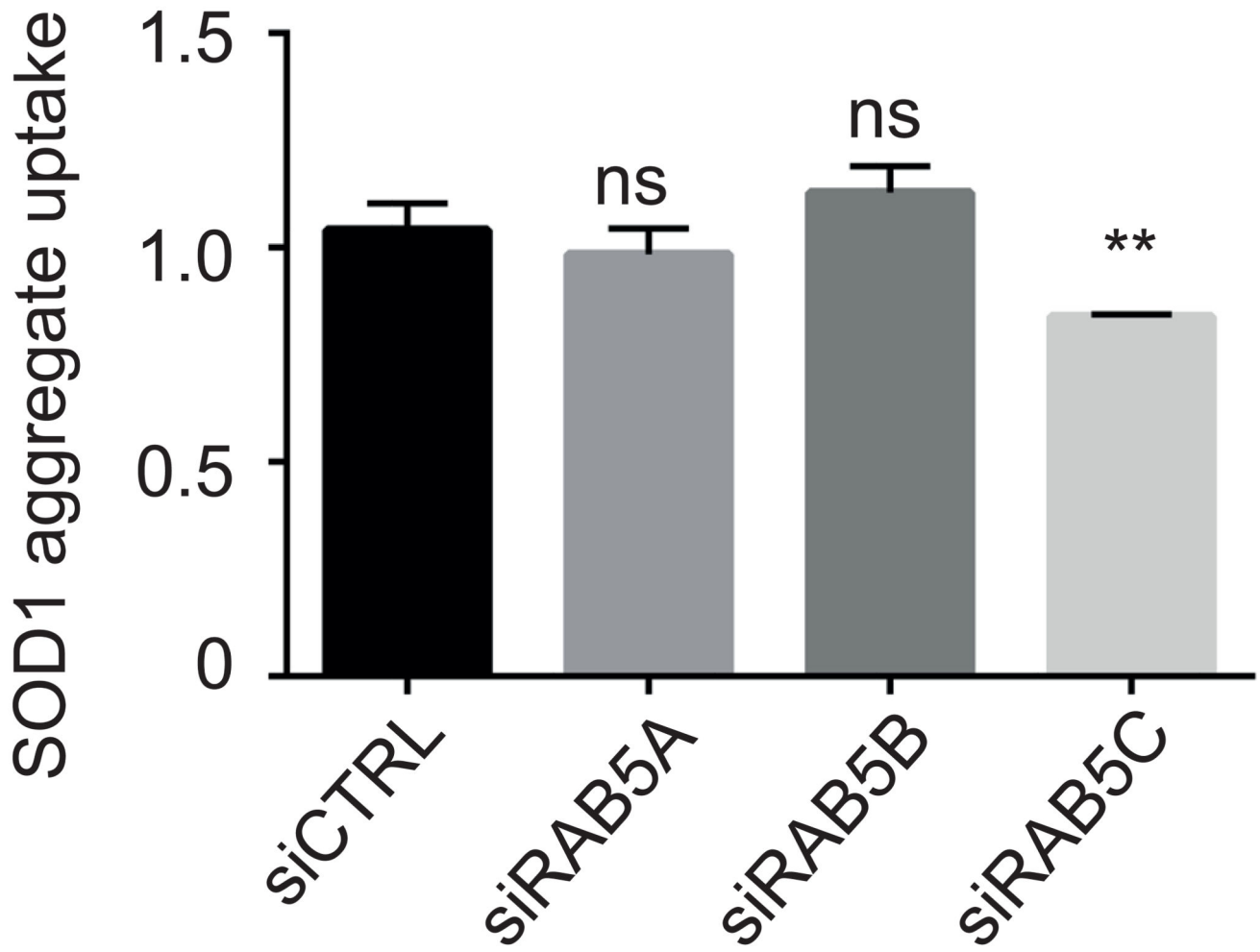

Figure EV6. SOD1 aggregate uptake following RAB5 knockdown.

Flow cytometry analysis of SK-N-AS cells 1 hour after inoculation with 0.8 μM Dylight650-SOD1^{H46R} aggregates and 3 days after transfection with the indicated siRNA. ** $P \leq 0.01$. Fluorescence intensity of was measured by flow cytometry on 10,000 cells per sample and analyzed by 0rdinary one-way ANOVA followed by multiple comparisons ($n \geq 2$).

Supplementary Material

Refer to Web version on PubMed Central for supplementary material.

Acknowledgements

We are grateful to Robin Ketteler, who provided a set of custom siRNAs, Cleo Bishop for advice on the screen design, Indrajit Das for SOD1 mice tissues, Yvonne Vallis for help with primary neurons and Arnaud Echard for discussions. This work was supported by the Medical Research Council (UK) MC-A023-5PD71, a Motor Neurone Disease Association grant (Bertolotti/Apr11/6072) and the European Research Council under the European Union's Seventh Framework Programme (FP7/2007-2013) / ERC grant 309516. A.B. is an honorary fellow of the Clinical Neurosciences Department of Cambridge University.

References

Ayers JI, Fromholt S, Koch M, DeBosier A, McMahon B, Xu G, Borchelt DR. Experimental transmissibility of mutant SOD1 motor neuron disease. Acta Neuropathol. 2014; 128:791–803. [PubMed: 25262000]

Ayers JI, Fromholt SE, O'Neal VM, Diamond JH, Borchelt DR. Prion-like propagation of mutant SOD1 misfolding and motor neuron disease spread along neuroanatomical pathways. Acta Neuropathol. 2015; 131:103–114. PubMed - NCBI. [PubMed: 26650262]

Berkova Z, Crawford SE, Blutt SE, Morris AP, Estes MK. Expression of Rotavirus NSP4 Alters the Actin Network Organization through the Actin Remodeling Protein Cofilin. Journal of Virology. 2007; 81:3545–3553. [PubMed: 17229686]

Brundin P, Melki R, Kopito R. Prion-like transmission of protein aggregates in neurodegenerative diseases. Nature Reviews Molecular Cell Biology. 2010; 11:301–307. [PubMed: 20308987]

Cossart P, Helenius A. Endocytosis of viruses and bacteria. Cold Spring Harbor Perspectives in Biology. 2014; 6 a016972–a016972.

Danzer KM, Haasen D, Karow AR, Moussaud S, Habeck M, Giese A, Kretzschmar H, Hengerer B, Kostka M. Different species of alpha-synuclein oligomers induce calcium influx and seeding. J Neurosci. 2007; 27:9220–9232. [PubMed: 17715357]

Das I, Krzyzosiak A, Schneider K, Wrabetz L, D'Antonio M, Barry N, Sigurdardottir A, Bertolotti A. Preventing proteostasis diseases by selective inhibition of a phosphatase regulatory subunit. Science. 2015; 348:239–242. [PubMed: 25859045]

Desplats P, Lee HJ, Bae EJ, Patrick C, Rockenstein E, Crews L, Spencer B, Masliah E, Lee SJ. Inclusion formation and neuronal cell death through neuron-to-neuron transmission of alpha-synuclein. Proc Natl Acad Sci USA. 2009; 106:13010–13015. [PubMed: 19651612]

Falcon B, Cavallini A, Angers R, Glover S, Murray TK, Barnham L, Jackson S, O'Neill MJ, Isaacs AM, Hutton ML, Szekeres PG, Goedert M, Bose S. Conformation determines the seeding potencies of native and recombinant Tau aggregates. J Biol Chem. 2015; 290:1049–1065. [PubMed: 25406315]

Frost B, Diamond MI. Prion-like mechanisms in neurodegenerative diseases. Nat Rev Neurosci. 2010; 11:155–159. [PubMed: 20029438]

Goedert M, Clavaguera F, Tolnay M. The propagation of prion-like protein inclusions in neurodegenerative diseases. Trends Neurosci. 2010; 33:317–325. [PubMed: 20493564]

Gowers, WR. Manual of Diseases of the Nervous System. Vol. VolumeI. LondonJ.&A.Churchill; 1892.

Grad LI, Guest WC, Yanai A, Pokrishevsky E, O'Neill MA, Gibbs E, Semenchenko V, Yousefi M, Wishart DS, Plotkin SS, Cashman NR. Intermolecular transmission of superoxide dismutase 1 misfolding in living cells. Proc Natl Acad Sci USA. 2011; 108:16398–16403. [PubMed: 21930926]

Grad LI, Yerbury JJ, Turner BJ, Guest WC, Pokrishevsky E, O'Neill MA, Yanai A, Silverman JM, Zeineddine R, Corcoran L, Kumita JR, et al. Intercellular propagated misfolding of wild-type Cu/Zn superoxide dismutase occurs via exosome-dependent and -independent mechanisms. Proc Natl Acad Sci USA. 2014; 111:3620–3625. [PubMed: 24550511]

Guerreiro R, Brás J, Hardy J. SnapShot: Genetics of ALS and FTD. Cell. 2015; 160:798–798.e1. [PubMed: 25679767]

Gurney ME, Pu H, Chiu AY, Dal Canto MC, Polchow CY, Alexander DD, Caliendo J, Hentati A, Kwon YW, Deng HX, et al. Motor neuron degeneration in mice that express a human Cu,Zn superoxide dismutase mutation. Science. 1994; 264:1772–1775. [PubMed: 8209258]

Holmes BB, DeVos SL, Kfoury N, Li M, Jacks R, Yanamandra K, Ouidja MO, Brodsky FM, Marasa J, Bagchi DP, Kotzbauer PT, et al. Heparan sulfate proteoglycans mediate internalization and propagation of specific proteopathic seeds. Proceedings of the National Academy of Sciences. 2013

Holzinger A. Jasplakinolide: an actin-specific reagent that promotes actin polymerization. Methods Mol Biol. 2009; 586:71–87. [PubMed: 19768425]

Johnston JA, Dalton MJ, Gurney ME, Kopito RR. Formation of high molecular weight complexes of mutant Cu, Zn-superoxide dismutase in a mouse model for familial amyotrophic lateral sclerosis. Proc Natl Acad Sci USA. 2000; 97:12571–12576. [PubMed: 11050163]

Jucker M, Walker LC. Pathogenic protein seeding in alzheimer disease and other neurodegenerative disorders. Ann Neurol. 2011; 70:532–540. [PubMed: 22028219]

Lappalainen P, Drubin DG. Cofilin promotes rapid actin filament turnover in vivo. Nature. 1997; 388:78–82. [PubMed: 9214506]

Liu L, Li J, Zhang L, Zhang F, Zhang R, Chen X, Brakebusch C, Wang Z, Liu X. Cofilin phosphorylation is elevated after F-actin disassembly induced by Rac1 depletion. Biofactors. 2015; 41:352–359. [PubMed: 26496994]

Liu L, Oliveira NM, Cheney KM, Pade C, Dreja H, Bergin A-MH, Borgdorff V, Beach DH, Bishop CL, Dittmar MT, McKnight Á. A whole genome screen for HIV restriction factors. Retrovirology. 2011; 8:94. [PubMed: 22082156]

Luh LM, Das I, Bertolotti A. qMotor, a set of rules for sensitive, robust and quantitative measurement of motor performance in mice. Nat Protoc. 2017; 12:1451–1457. [PubMed: 28686587]

Maekawa M, Ishizaki T, Boku S, Watanabe N, Fujita A, Iwamatsu A, Obinata T, Ohashi K, Mizuno K, Narumiya S. Signaling from Rho to the actin cytoskeleton through protein kinases ROCK and LIM-kinase. Science. 1999; 285:895–898. [PubMed: 10436159]

Mizuno K. Signaling mechanisms and functional roles of cofilin phosphorylation and dephosphorylation. Cellular Signalling. 2013; 25:457–469. [PubMed: 23153585]

Mizuno K, Yang N, Higuchi O, Ohashi K, Nagata K, Wada A, Kangawa K, Nishida E. Cofilin phosphorylation by LIM-kinase 1 and its role in Rac-mediated actin reorganization. Nature. 1998; 393:809–812. PubMed - NCBI. [PubMed: 9655398]

Munch C, Bertolotti A. Propagation of the prion phenomenon: beyond the seeding principle. J Mol Biol. 2012; 421:491–498. [PubMed: 22245492]

Murray IVJ, Giasson BI, Quinn SM, Koppaka V, Axelsen PH, Ischiropoulos H, Trojanowski JQ, Lee VM-Y. Role of α-Synuclein Carboxy-Terminus on Fibril Formation in Vitro †. Biochemistry. 2003; 42:8530–8540. [PubMed: 12859200]

Münch C, O'Brien J, Bertolotti A. Prion-like propagation of mutant superoxide dismutase-1 misfolding in neuronal cells. Proc Natl Acad Sci U S A. 2011; 108:3548–3553. [PubMed: 21321227]

Nagata-Ohashi K, Ohta Y, Goto K, Chiba S, Mori R, Nishita M, Ohashi K, Kousaka K, Iwamatsu A, Niwa R, Uemura T, et al. A pathway of neuregulin-induced activation of cofilin-phosphatase Slingshot and cofilin in lamellipodia. The Journal of Cell Biology. 2004; 165:465–471. [PubMed: 15159416]

Prusiner SB. Prions. Proc Natl Acad Sci U S A. 1998; 95:13363–13383. [PubMed: 9811807]

Prusiner SB. Cell biology. A unifying role for prions in neurodegenerative diseases. Science. 2012; 336:1511–1513. [PubMed: 22723400]

Ravits JM, La Spada AR. ALS motor phenotype heterogeneity, focality, and spread: deconstructing motor neuron degeneration. Neurology. 2009; 73:805–811. [PubMed: 19738176]

Sanders DW, Kaufman SK, DeVos SL, Sharma AM, Mirbaha H, Li A, Barker SJ, Foley AC, Thorpe JR, Serpell LC, Miller TM, et al. Distinct tau prion strains propagate in cells and mice and define different tauopathies. Neuron. 2014; 82:1271–1288. [PubMed: 24857020]

Sibilla C, Bertolotti A. Prion Properties of SOD1 in Amyotrophic Lateral Sclerosis and Potential Therapy. Cold Spring Harbor Perspectives in Biology. 2017; 9

Sivadasan R, Hornburg D, Drepper C, Frank N, Jablonka S, Hansel A, Lojewski X, Sterneckert J, Hermann A, Shaw PJ, Ince PG, et al. C9ORF72 interaction with cofilin modulates actin dynamics in motor neurons. Nat Neurosci. 2016:1–12.

Soosairajah J, Maiti S, Wiggan O, Sarmiere P, Moussi N, Sarcevic B, Sampath R, Bamburg JR, Bernard O. Interplay between components of a novel LIM kinase-slingshot phosphatase complex regulates cofilin. EMBO J. 2005; 24:473–486. [PubMed: 15660133]

Soto C. Unfolding the role of protein misfolding in neurodegenerative diseases. Nat Rev Neurosci. 2003; 4:49–60. [PubMed: 12511861]

Thomas EV, Fenton WA, McGrath J, Horwich AL. Transfer of pathogenic and nonpathogenic cytosolic proteins between spinal cord motor neurons in vivo in chimeric mice. Proceedings of the National Academy of Sciences. 2017; 114:E3139–E3148.

Wang J, Farr GW, Zeiss CJ, Rodriguez-Gil DJ, Wilson JH, Furtak K, Rutkowski DT, Kaufman RJ, Ruse CI, Yates JR, Perrin S, et al. Progressive aggregation despite chaperone associations of a mutant SOD1-YFP in transgenic mice that develop ALS. Proc Natl Acad Sci U S A. 2009; 106:1392–1397. [PubMed: 19171884]

Westergard T, Jensen BK, Wen X, Cai J, Kropf E, Iacovitti L, Pasinelli P, Trotti D. Cell-to-Cell Transmission of Dipeptide Repeat Proteins Linked to C9orf72-ALS/FTD. CellReports. 2016; 17:645–652.

Wu C-H, Fallini C, Ticozzi N, Keagle PJ, Sapp PC, Piotrowska K, Lowe P, Koppers M, McKenna-Yasek D, Baron DM, Kost JE, et al. Mutations in the profilin 1 gene cause familial amyotrophic lateral sclerosis. Nature. 2012; 488:499–503. [PubMed: 22801503]

Xiang Y, Zheng K, Ju H, Wang S, Pei Y, Ding W, Chen Z, Wang Q, Qiu X, Zhong M, Zeng F, et al. Cofilin 1-mediated biphasic F-actin dynamics of neuronal cells affect herpes simplex virus 1 infection and replication. J Virol. 2012; 86:8440–8451. [PubMed: 22623803]

Yerbury JJ. Protein aggregates stimulate macropinocytosis facilitating their propagation. Prion. 2016; 10:119–126. [PubMed: 26963158]

Yoder A, Yu D, Dong L, Iyer SR, Xu X, Kelly J, Liu J, Wang W, Vorster PJ, Agulto L, Stephany DA, et al. HIV Envelope-CXCR4 Signaling Activates Cofilin to Overcome Cortical Actin Restriction in Resting CD4 T Cells. Cell. 2008; 134:782–792. [PubMed: 18775311]

Zeineddine R, Pundavela JF, Corcoran L, Stewart EM, Do-Ha D, Bax M, Guillemin G, Vine KL, Hatters DM, Ecroyd H, Dobson CM, et al. SOD1 protein aggregates stimulate macropinocytosis in neurons to facilitate their propagation. Molecular Neurodegeneration. 2015:1–18. [PubMed: 25567526]

Zheng K, Xiang Y, Wang Q, Zhong M, Wang S, Wang X, Fan J, Kitazato K, Wang Y. Epidermal growth factor receptor-PI3K signaling controls cofilin activity to facilitate herpes simplex virus 1 entry into neuronal cells. mBio. 2013; 5 PubMed - NCBI e00958–13–e00958–13.

Europe PMC Funders Author Manuscripts

Europe PMC Funders Author Manuscripts

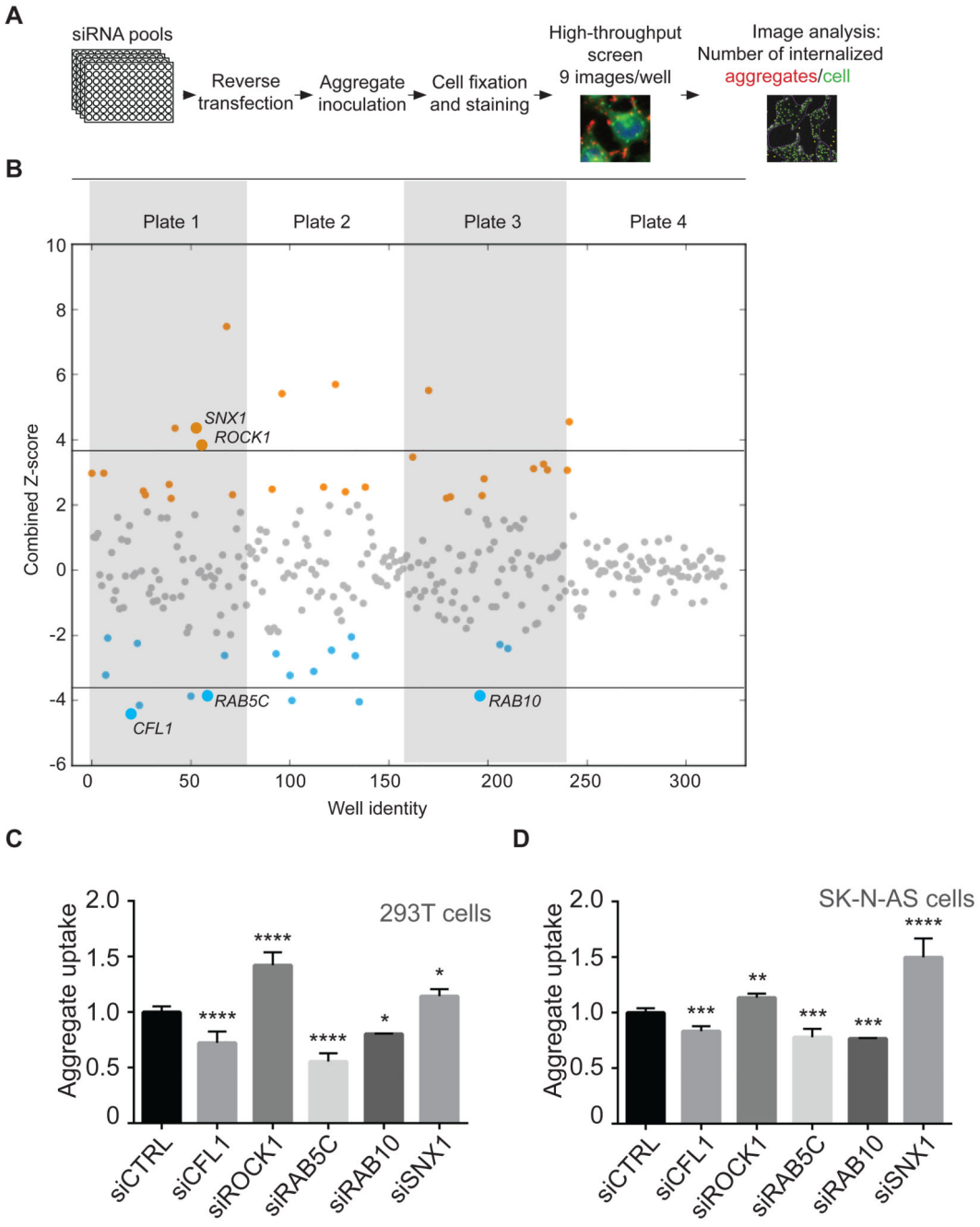

Figure 1. An unbiased high-content screen identifies modifiers of aggregate entry.

A. Scheme representing the experimental workflow.

B. Combined *Z*-scores for each siRNA knockdown or mock transfection, presented as a scatter plot with the X-axis indicating the screening well. *Z*-score points representing hits above 2.0 are colored in orange and below -2 in blue. Horizontal lines illustrate the *Z*-score threshold (±3.8) used for the secondary screen, selecting 15 of the most significant candidate genes.

C. Flow cytometry analysis of 293T cells 16 hours after inoculation with 0.8 μM Dylight650-SOD1^{H46R} aggregates. Cells were transfected with the indicated siRNA or control (CTRL) siRNA 3 days before their inoculation with aggregates. Fluorescence intensity of aggregates was measured by flow cytometry on 10,000 cells per sample (n=2-5) and results were analyzed by ordinary one-way ANOVA followed by multiple comparisons.
D. Flow cytometry analysis of SK-N-AS cells 1 hour after inoculation with 0.8 μM Dylight650-SOD1^{H46R} aggregates and 3 days after transfection with the indicated siRNA. Fluorescence intensity of was measured by flow cytometry on 10,000 cells per sample (n=3-10) results were analyzed by ordinary one-way ANOVA followed by multiple comparisons.
C, D. Data are means ± SEM *$P \leq 0.05$, **$P \leq 0.01$. ***$P \leq 0.001$. ****$P \leq 0.0001$.

Europe PMC Funders Author Manuscripts

Europe PMC Funders Author Manuscripts

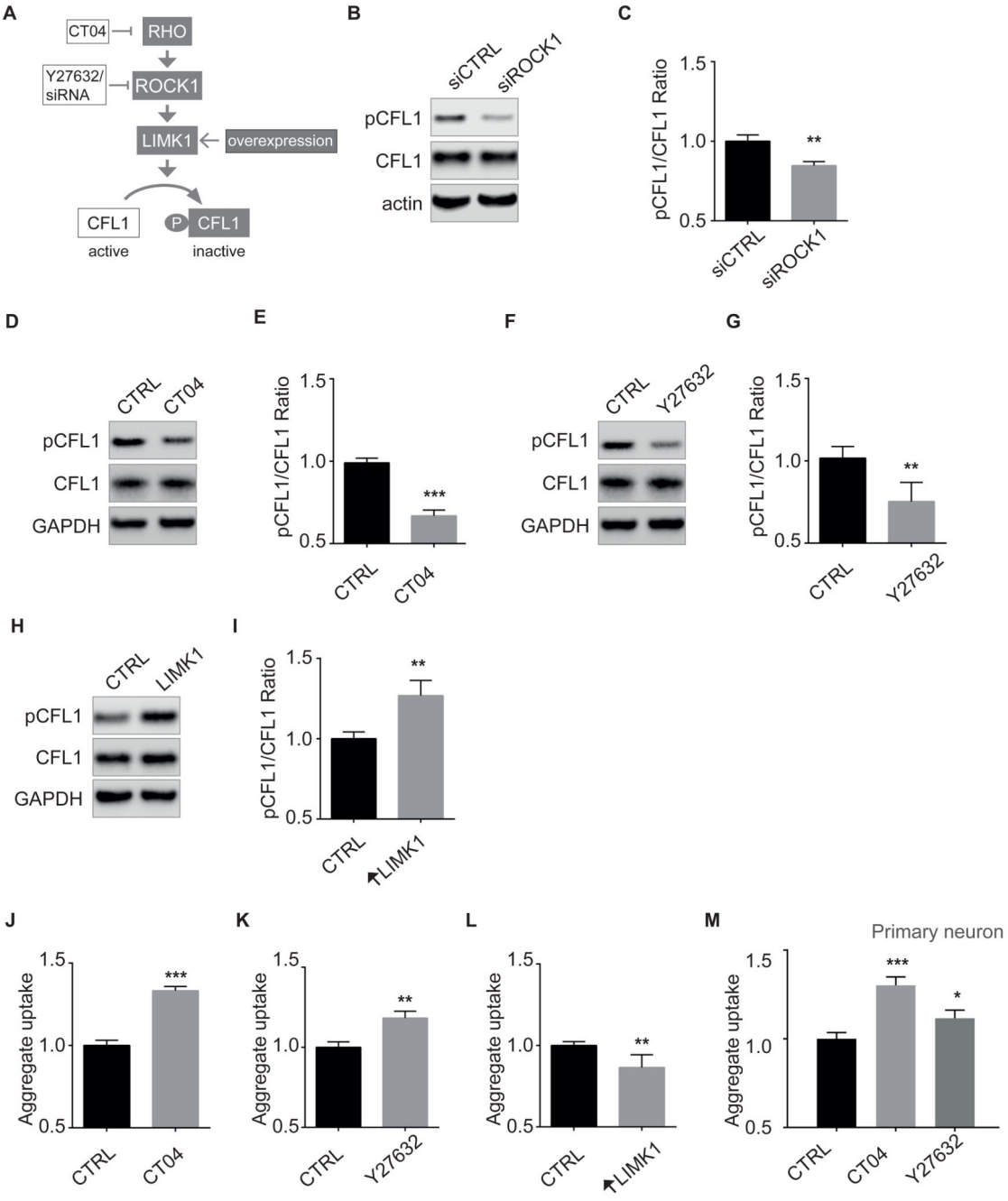

Figure 2. Signaling from RHO to cofilin-1 controls aggregate entry into cells.

A. Cartoon depicting the RHO-ROCK1, LIMK1 signaling pathway to cofilin-1 (CFL1).

B. Immunoblots of the indicated proteins in lysates of SK-N-AS cells 3 days after transfection with ROCK1 siRNA or control siRNA.

C. Quantifications of triplicates of (B). The graph depicts levels of pCFL1 relative to total CFL1 in cells with ROCK1 siRNA knockdown compared with control siRNA treatment. Data are means ± SEM ($n = 3$). Unpaired t test. Two tailed p = 0.0043.

D. Immunoblots of the indicated proteins in lysates of SK-N-AS cells treated with CT04 or vehicle (CTRL).

E. Quantifications of replicates of (D). Data are means ± SEM ($n = 3$). Unpaired *t* test. Two tailed p = 0.0003.

F, **G**. Same as (D, E) with Y27632. Data are means ± SEM ($n = 4$). Unpaired *t* test. Two tailed p = 0.0081.

H. Immunoblots of the indicated proteins in lysates of SK-N-AS cells 2 days after transfection with pTGSH-LIMK1 or empty vector.

I. Quantifications of replicates of (H). Data are means ± SEM ($n = 4$). Unpaired *t* test. Two tailed p = 0.0021.

J, **K**. Flow cytometry analysis of SK-N-AS cells 1 hour after inoculation with 0.8 μM Dylight650-SOD1^{H46R} aggregates and following a 15 hours treatment with 1μg/ml CT04 (J) or 10 μM Y27632 (K) or vehicle (CTRL). Data are means ± SEM ($n = 3$). Unpaired *t* test. Two tailed p values are 0.0001 and 0.0097 with treatment of CT04 and Y27632, respectively.

L. Flow cytometry analysis of aggregates uptake in SK-N-AS cells transfected with pTGSH-LIMK1 or empty vector as a control 2 days before inoculation with labelled SOD1 aggregates. Data are means ± SEM ($n = 3$). Unpaired *t* test. Two tailed p = 0.0064.

M. Flow cytometry analysis of aggregates uptake 1 hour after inoculation of aggregates in primary neuron in the presence of 1 μg/ml CT04 or 10 μM Y27632 or vehicle (CTRL) added 1 hour before aggregates. Data are means ± SEM ($n = 3$). Unpaired *t* test. Two tailed p values are 0.0009 and 0.0254 with treatment of CT04 and Y27632, respectively.

B, D, F, H Representative results are shown. J, K, L, M. Fluorescence intensity of was measured by flow cytometry on 10,000 cells per sample on a LSRFortessaTM (BD Biosciences). *$P \leq 0.05$, **$P \leq 0.01$. ***$P \leq 0.001$.

Europe PMC Funders Author Manuscripts

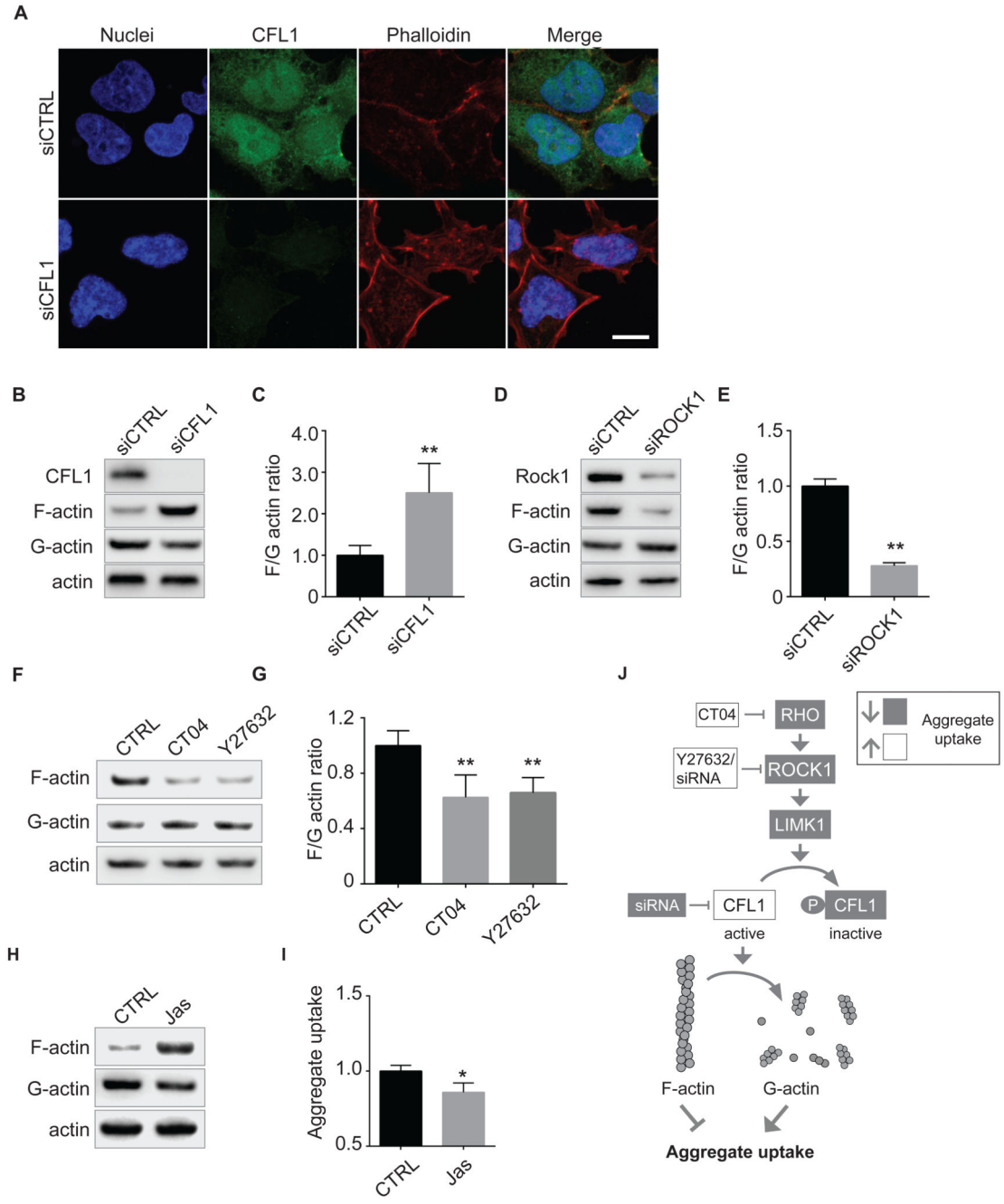

Figure 3. Cofilin-1 controls cortical actin, a barrier to SOD1 aggregates entry.

A. Confocal images of 293T cells 3 days after transfection with cofilin-1 (CFL1) siRNA or control siRNA and stained with H33342 (blue) to reveal nuclei, anti-CFL1 antibody (green) and phalloidin (red) to reveal actin filaments. Scale bar: 10 μM.

B. Fractionation of cell lysates followed by immunoblots to reveal F-actin, G-actin. SK-N-AS cells were transfected with control or CFL1 siRNA 3 days before the analysis.

Europe PMC Funders Author Manuscripts

C. Quantifications of replicates of (B). The graph depicts levels of F-actin/G-actin ratios in cells transfected with or without CFL1 siRNA. Data are means ± SEM ($n = 4$). Unpaired t test. Two tailed p =0.0068.

D, **E**. As in (B, C) except that cells were transfected with control or ROCK1 siRNA. Data are means ± SEM ($n = 2$). Unpaired t test. Two tailed p =0.0046.

F. Fractionation of SK-N-AS cell lysates followed by immunoblots to reveal F-actin, G-actin. Before lysis, cells were treated for 16 hours with 1μg/ml CT04 or 10 μM Y27632.

G. Quantification of replicated experiments as in (F). Data are means ± SEM ($n = 4$). Unpaired t test. Two tailed p values are 0.0083 and 0.0043 with treatment of CT04 and Y27632, respectively.

H. Immunoblots of F-actin, G-actin and total actin in fractionated lysates from SK-N-AS cells after a treatment with vehicle (DMSO) or 25nM Jasplakinolide for 16 hours.

I. Flow cytometry analysis of aggregates entry, 1 hour after inoculation of SK-N-AS cells with 0.8 μM Dylight650-SOD1^{H46R} aggregates following a treatment with vehicle (DMSO) or 25nM Jasplakinolide for 16 hours. Fluorescence intensity of was measured by flow cytometry on 10,000 cells per sample ($n = 2$). Data are means ± SEM. Unpaired t test. Two tailed p=0.0155.

J. Cartoon depicting the regulation of acting remodeling by the RHO to CFL1 pathway.

A. B. D. H Representative results are shown. C, E, G, I. *$P \leq 0.05$, **$P \leq 0.01$.

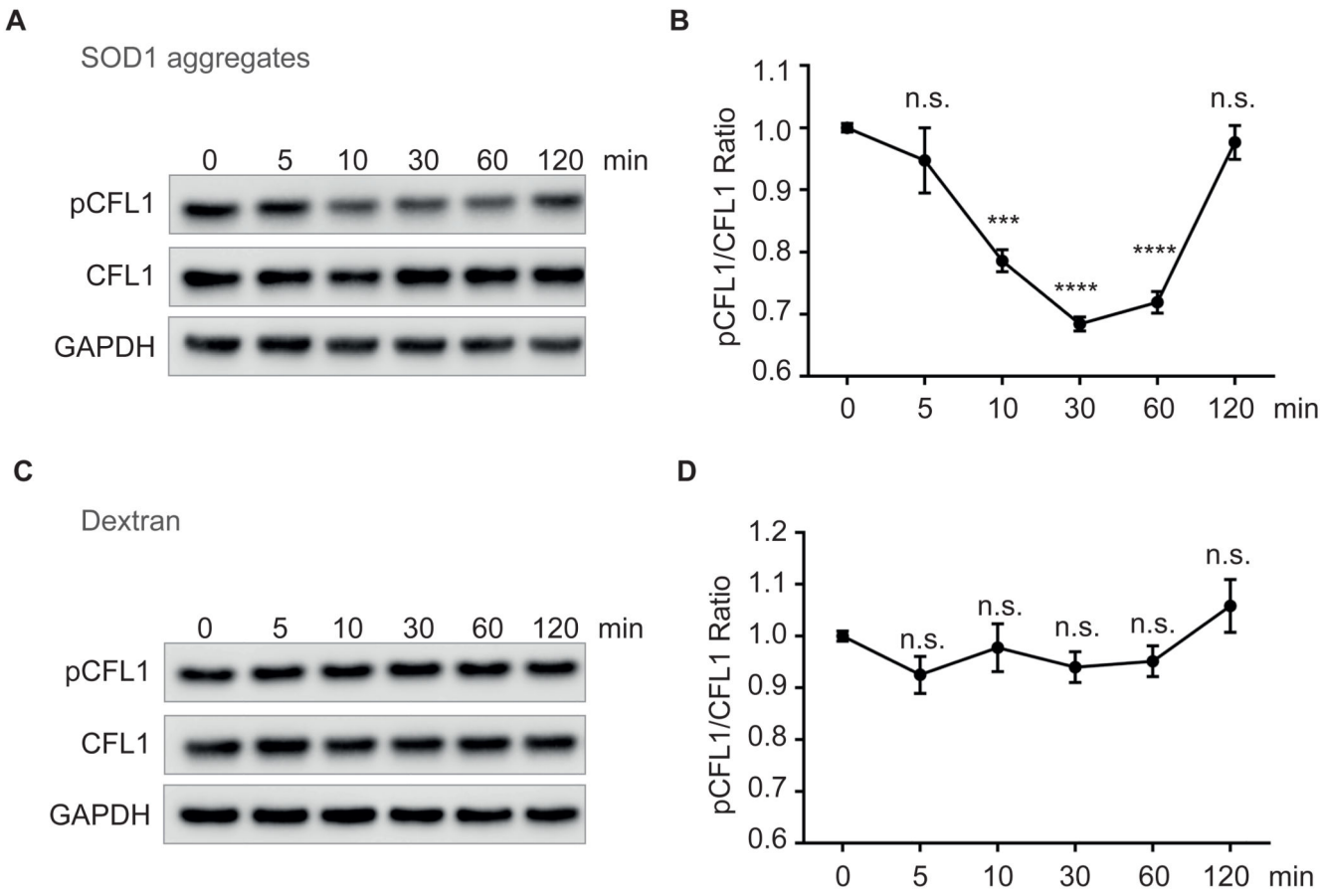

Figure 4. SOD1 aggregates transiently alter cofilin-1 phosphorylation in cells.

A. Immunoblots of the indicated proteins in lysates of SK-N-AS cells inoculated with SOD1 aggregates for the indicated time.

B. Quantifications of triplicates of (A). The graph depicts the level of pCFL1 relative to total CFL1 during the SOD1 aggregates inoculation in SK-A-AS cells. Ordinary one-way ANOVA followed by multiple comparisons (n=3).

C. SK-N-AS cells inoculated with Dextran (Mr 10,000) for the indicated time were lysed and analysed by immunoblots with the indicated antibodies.

D. Quantifications of triplicates of (C). The graph depicts the level of pCFL1 relative to total CFL1 during the Dextran (Mr 10,000) inoculation in SK-A-AS cells. Ordinary one-way ANOVA followed by multiple comparisons (n=3).

A, C. Representative results are shown. B, D. n.s.: P >0.05, ***$P \leq 0.001$. ****$P \leq 0.0001$.

Europe PMC Funders Author Manuscripts

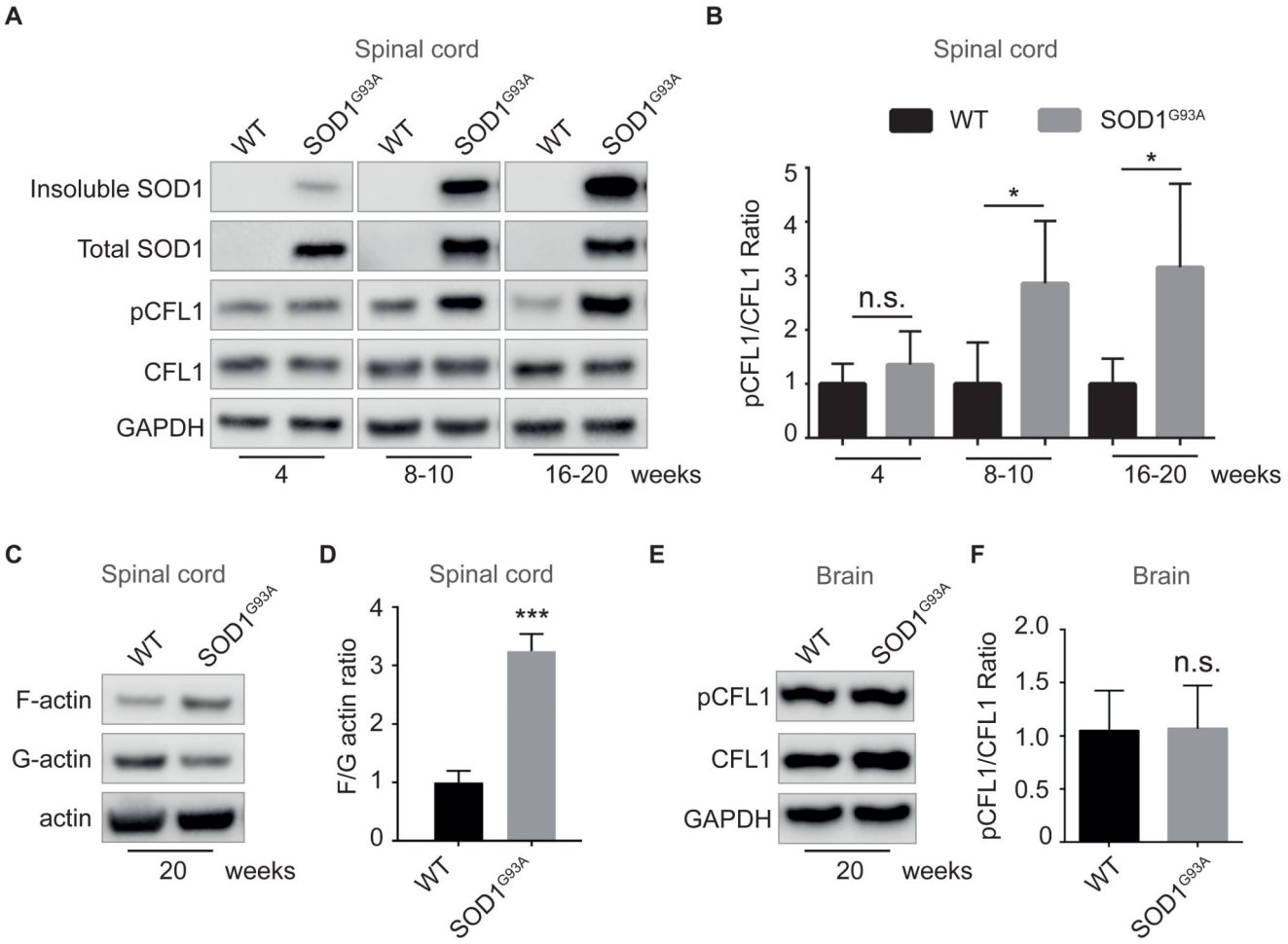

Figure 5. SOD1 aggregates alter cofilin-1 phosphorylation in SOD1^{G93A} transgenic mice.

A. Immunoblots of the indicated proteins in spinal cord lysates of SOD1^{G93A} transgenic mice or wild-type mice from 4 weeks to 20 weeks of age.

B. Quantifications of the pCFL1/CFL1 ratio in immunoblots such as the ones shown in (A). The graph depicts levels of pCFL1 relative to total CFL1 in lumbar region of the spinal cord of SOD1^{G93A} compared with wild-type. Data are means ± SEM (n = 3). Unpaired t test. Two tailed p values are 0.2359, 0.0363 and 0.0376 in each age group separately.

C. Actin fractionation followed by immunoblots of spinal cord lysates from SOD1^{G93A} transgenic or wild-type mice (20 weeks old).

D. Quantifications of the F-actin/G-actin ratios on immunoblots as in (C). The graph depicts the level of F-actin/G-actin ratios in lumbar region of the spinal cord of SOD1^{G93A} compared with wild-type at 20 weeks. Data are means ± SEM (n = 3). Unpaired t test. Two tailed p =0.0004.

E. Immunoblots of the indicated proteins in whole brain lysates of SOD1^{G93A} transgenic or wild-type mice (20 weeks old).

F. Quantifications of the pCFL1/CFL1 ratio on immunoblots as in (E). The graph depicts the level of pCFL1 relative to total CFL1 in brains of SOD1^{G93A} compared with wild-type at 20 weeks. Data are means ± SEM (n = 5). Unpaired t test. Two tailed p =0.8644.

A, C and E. Representative results are shown. B, D and F. n.s.: not significant. P>0.05, *P≤0.05, ***P≤0.001.

Europe PMC Funders Author Manuscripts

Europe PMC Funders Author Manuscripts

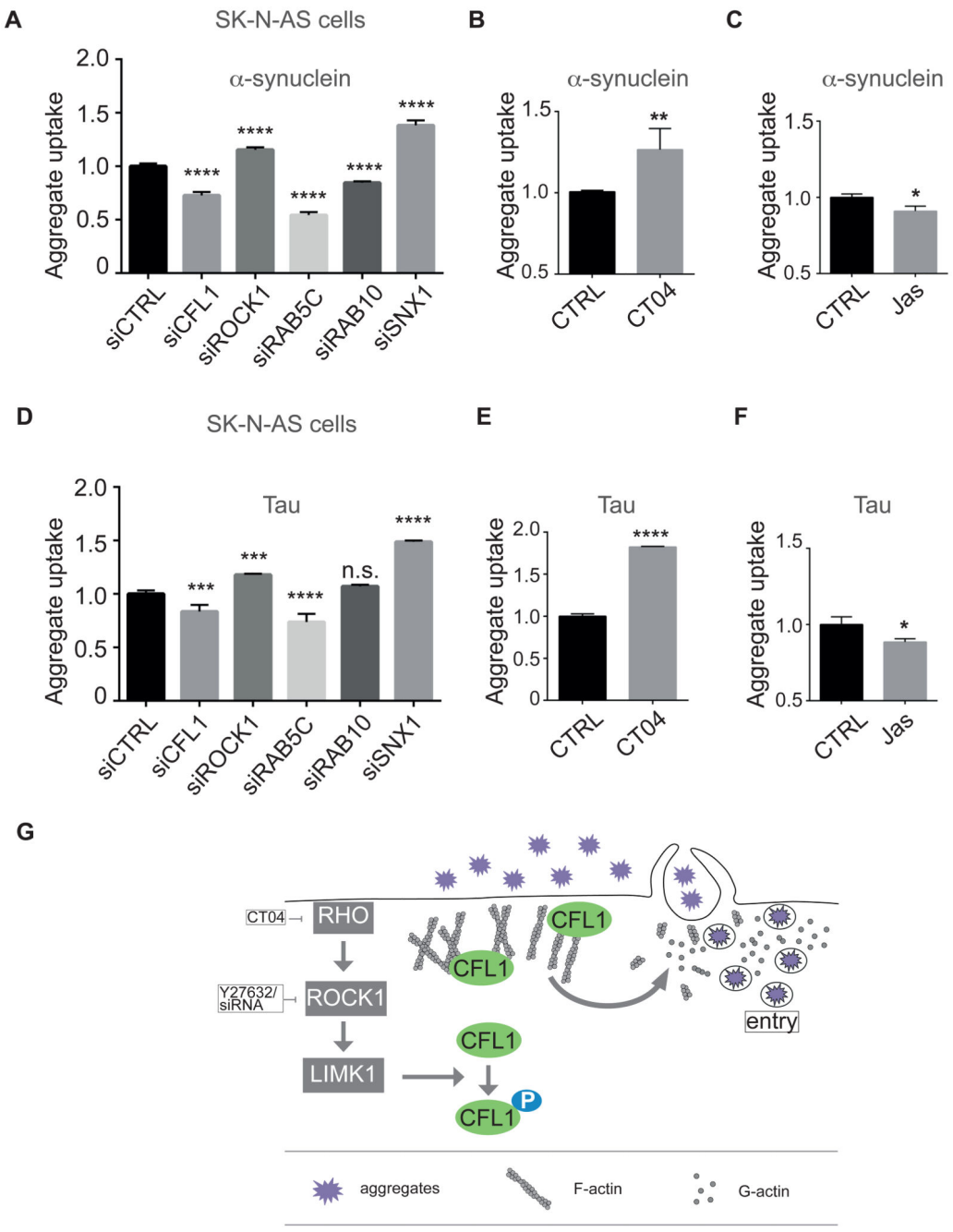

Figure 6. The RHO to cofilin-1 signaling pathway modulates entry of diverse protein aggregates.

A. Flow cytometry analysis of aggregates entry after inoculation of SK-N-AS cells with 0.1 μM Dylight650-α-synuclein aggregates and 3 days after transfection with the indicated siRNA. Fluorescence intensity of was measured by flow cytometry on 10,000 cells per sample (n=3). Ordinary one-way ANOVA followed by multiple comparisons.

B, **C**. Flow cytometry analysis of α-synuclein aggregates uptake as in (A) except that SK-N--AS cells were treated with 1 μg/ml CT04 (B) or 25 nM Jasplakinolide (C) for 16 hours. Data

are means ± SEM (n = 3). Unpaired t test. Two tailed p values are 0.0073 and 0.0159 with treatment of CT04 and Jasplakinolide, respectively.

D. Flow cytometry analysis of SK-N-AS cells after inoculation with 0.06 μM Dylight650--tau aggregates and 3 days after transfection with the indicated siRNA. Fluorescence intensity of was measured by flow cytometry on 10,000 cells per sample (n=3). Ordinary one-way ANOVA followed by multiple comparisons.

E, **F**. Same as in (B and C) with tau aggregates. Data are means ± SEM. (n≥3). *P≤0.05, ** P≤0.01, *** P≤0.001, ***P≤0.0001. Representative results are shown. Data are means ± SEM (n = 3). Unpaired t test. Two tailed p values are 0.0001 and 0.0232 with treatment of CT04 and Jasplakinolide, respectively.

G. The Rho to cofilin-1 signaling pathway is exploited by protein aggregates to remodel to cortical actin, enabling cell entry.

A-F Fluorescence intensity of was measured by flow cytometry on 10,000 cells per sample on a LSRFortessaTM (BD Biosciences). *P≤0.05, ** P≤0.01, *** P≤0.001, ***P≤0.0001.

Europe PMC Funders Author Manuscripts